

## On equivalent hydraulic conductivity for oscillation-free solutions of Richard's equation



Benjamin Belfort\*, Anis Younes, Marwan Fahs, François Lehmann

Laboratoire d'Hydrologie et de Géochimie de Strasbourg, Université de Strasbourg, CNRS/UMR 7517, 1 rue Blessig, F-67084 Strasbourg, France

### ARTICLE INFO

#### Article history:

Received 29 April 2013

Received in revised form 12 September 2013

Accepted 26 September 2013

Available online 4 October 2013

This manuscript was handled by Corrado Corradini, Editor-in-Chief, with the assistance of Aldo Fiori, Associate Editor

#### Keywords:

Numerical methods

Unsaturated flow

Richards' equation

Internodal conductivity

Mass-lumping

Monotonicity

### ABSTRACT

The estimation of numerical equivalent conductivity remains a crucial issue for the accuracy and stability of the solution of the non-linear Richards' equation (RE) when modeling variably saturated flow. In the literature, it appears that this topic has been typically considered for one-dimensional discretization despite the growing interest in multidimensional problems. After reviewing different possibilities of equivalent hydraulic conductivity estimation, we evaluate their ability to yield monotonic results. Hence, the monotonicity analysis provided by Forsyth and Kropinski (1997) has been generalized for the different equivalent conductivity formulations. On one hand, the upstream mean is unconditionally stable but is also known to overestimate the conductivity. On the other hand, other formulations, including Darcian mean approximations, can be accurate and straightforward to adapt in multidimensional codes but do not always provide monotonic solutions of the RE. An adaptive algorithm is presented, which adapts the conductivity in function of the monotonicity condition, i.e., a variable criterion based on the conductivity at nodal points, the conductivity averaging technique and the piezometric head variation. The proposed numerical method can be implemented in existing multidimensional codes. Numerical investigations in steady state and time-varying conditions, 1D and 2D cases, and homogeneous and heterogeneous media confirm the interest in the proposed algorithm.

© 2013 Elsevier B.V. All rights reserved.

### 1. Introduction

Modeling water flow in variably saturated soils is of great interest to many scientific research and engineering applications involved in the management of water resources. Richards' equation (1931) (RE) has been described as a valuable model to predict water movement in variably saturated media and to provide inputs for contaminant transport models (Šimůnek and Bradford, 2008). The development of robust and fast numerical simulators for unsaturated flow remains a challenging research subject of research (Crevoisier et al., 2009; Kuráž et al., 2010; Wu, 2010; An et al., 2011; Zadeh, 2011; Lott et al., 2012; Zambra et al., 2012). In fact, when simulating unsaturated flow in porous media, numerical oscillations may occur when the spatial distribution or temporal evolution of the pressure head or water content fluctuate around the correct value. Traditionally, the issue of oscillation is typically raised for methods based on variational formulation, such as finite element (FE) (Neuman, 1972; Sandhu et al., 1977; Vermeer and Verruijt, 1981; Milly, 1985; Celia et al., 1990; Pan et al., 1996; Wood, 1996; Thomas and Zhou, 1997; Karthikeyan et al., 2001). Many studies dealing with RE focus on the numerical

expression of the mass matrix for time-dependent problems and conclude that the diagonalized (or lumped) form is preferred to avoid oscillations (Neuman, 1972; Cooley, 1983; Milly, 1985; Celia et al., 1990; Pan et al., 1996; Ju and Kung, 1997). In this context, the M-matrix property (i.e., a non-singular matrix with positive diagonal and negative off-diagonal coefficients) is often used to establish conditions that ensure consideration of the maximum principle (Windisch, 1989; Wood, 1996; Thomas and Zhou, 1997; Hoteit et al., 2002; Belfort and Lehmann, 2005; Younes et al., 2006). This suitable mathematical property prevents unrealistic results in the case of saturated flow but is not sufficient for unsaturated flow (e.g., Forsyth and Kropinski, 1997).

However, the behavior of the solution is dependent on the equivalent conductivity ( $K_{eq}$ ) used in the numerical method for the spatial discretization of RE.  $K_{eq}$  represents the mean value of the hydraulic conductivity related to Darcy–Buckingham's law and is calculated between two cells or control volumes for finite difference (FD) and finite volume (FV) methods (Haverkamp and Vauclin, 1979; Schnabel and Richie, 1984; Warrick, 1991; Zaidel and Russo, 1992; Baker, 1995; Romano et al., 1998; Gastó et al., 2002; Brunone et al., 2003), or inside the element for finite element (FE) and mixed hybrid finite element (MHFE) methods (Farthing et al., 2003; Belfort and Lehmann, 2005). Previous studies consider the relation between a formulation of equivalent conductivity and

\* Corresponding author. Tel.: +33 368 850 386; fax: +33 368 850 402.  
E-mail address: [belfort@unistra.fr](mailto:belfort@unistra.fr) (B. Belfort).

the accuracy of the numerical solution. In fact, studies have been found whose authors recommended the use of the geometric mean (e.g., Haverkamp and Vauclin, 1979), arithmetic mean (van Dam and Feddes, 2000), harmonic mean (Oldenburg and Pruess, 1993), upstream mean (Oldenburg and Pruess, 1993), integrated mean (Pei et al., 2012), or more complex averages, such as the Darcian mean (Warrick, 1991; Baker, 1995) or optimized algorithm (Szymkiewicz, 2009). A review on averaging approaches for the computation of inter-nodal permeabilities is given in the chapter 4 of the book by Szymkiewicz (2013). Based on many studies on the subject, it appears that a single simple average could never be adapted for the various combinations of soil materials, spatial grid sizes and water flow conditions. Additionally, the difficulty in incorporating soil heterogeneity in the estimation of the hydraulic conductivity has been studied, typically for the one-dimensional FD method (e.g., Romano et al., 1998; Szymkiewicz and Helmig, 2011).

Only a few authors consider the  $K_{eq}$  selection to avoid oscillations (Baker et al., 1999; Forsyth and Kropinski, 1997; van Dam and Feddes, 2000; Baker, 2006; Szymkiewicz, 2009). Among the different methods, it has been shown that the Darcian mean approximations produce accurate results (Warrick, 1991; Baker, 2006; Szymkiewicz, 2009). However, Darcian mean approximations generally require numerical efforts to be implemented into existing codes, cannot always accept specific relationships describing retention and conductivity and their extension to multidimensional cases with complex geometries remains a challenging issue.

This study focuses on the numerical solution of water flow problems described by the standard RE, i.e., rigid porous media are considered and infinite air phase mobility is assumed. Because monotonicity constitutes the central issue of the paper, other significant research areas, such as linearization strategy (Lott et al., 2012), non-equilibrium and dynamic effect (Schweizer, 2012) are not investigated. Nonetheless, it should be noted that the results obtained in the current study could be applied to a large variety of numerical codes dealing with variably saturated flow problems.

The main objectives of this study are as follows: (1) review the different estimations of equivalent conductivity, (2) analyze their ability to yield monotonic results from a mathematical viewpoint, (3) test a new switching algorithm for a multidimensional implementation and (4) study the efficiency of the different averaging techniques by considering several 1D and 2D test cases.

## 2. Unsaturated flow modeling

The mathematical model used to describe the physical problem of water flow in unsaturated soil is given by the combination of Eqs. (1) and (2). Darcy–Buckingham’s law defines the water flux in the domain as follows:

$$q = -K(h) \cdot \nabla H \quad (1)$$

where  $q$  is the macroscopic fluid flux density [ $L T^{-1}$ ];  $K$  is the hydraulic conductivity [ $L T^{-1}$ ]; and  $H$  [L] and  $h$  [L] are the piezometric and pressure head, respectively, such that  $H = h + z$ , where  $z$  is the depth with upward being positive [L]. The mass conservation of water, under the assumption of incompressible media and fluid, leads to the mixed form of RE as follows:

$$\frac{\partial \theta}{\partial t} + \nabla \cdot q = f \quad (2)$$

where  $\theta$  is the volumetric water content [ $L^3 L^{-3}$ ];  $t$  is the time [T];  $f$  is a source/sink term [ $T^{-1}$ ]; and  $q$  is the previously defined water flux.

To solve the governing flow equations, initial and boundary conditions should be specified. Moreover, the interdependencies of  $h$ ,  $\theta$  and  $K$  should be characterized using constitutive relations

(often exponential or power functions). Table 1 summarizes different relative conductivity functions, such as  $K(h) = K_s \times K_r(h)$ , and the referred effective saturation (Se) [–] is defined by  $Se = \frac{\theta - \theta_r}{\theta_s - \theta_r}$ .  $K_s$  is the saturated conductivity [ $L T^{-1}$ ], which in general may be a tensor, and  $\theta_s$  [ $L^3 L^{-3}$ ] and  $\theta_r$  [ $L^3 L^{-3}$ ] are the saturated and residual volumetric water contents, respectively.

As reported in literature and depending on the problem considered, specific storage coefficients can be included in the RE to account for fluid compressibility and solid matrix deformability. Additionally, several forms of RE found with either the water content and/or pressure head as the main variable, requiring specific attention when expressing the capillary capacity (Celia et al., 1990; Rathfelder and Abriola, 1994). Because the main objective of this study is not dependent upon the precise form of the RE, only the mixed form (Eq. (2)) will be considered.

## 3. Numerical resolution of Richards’ equation

### 3.1. Presentation of numerical methods

When numerical methods are used to solve a physical problem modeled by the RE, the differential equation is integrated over the solution domain  $\Omega$ , which is decomposed into a set of non-overlapping smaller subdomains  $\Omega_e$  (such as  $\Omega = \bigcup \Omega_e$ ). The unknown variables and dependent coefficient are generally approximated at nodal points for FE or at the center of each control volume for FD and FV. The MHFE method uses both cell, and nodal (1D)/edge (2D) or face (3D) averaged values. Regardless of the method chosen, the final matrix system has the form:

$$[A] \cdot \{H\}_x + [B] \cdot \left\{ \frac{\partial \theta}{\partial t} \right\}_x - \{F\}_x = \{0\} \quad (3)$$

where  $x$  is a node (FE), cell (FD, FV) or face/edge (lumped MHFE) indice. Matrices  $[A]$  and  $[B]$  consist of the spatial and temporal approximations obtained from the numerical approximation on each subdomain,  $[A] = \sum_e [A^e]$  and  $[B] = \sum_e [B^e]$ , respectively. It should be noted that  $\{F\}$  contains sink/source terms and boundary conditions. The  $i$ th ordinary differential equation, referred to as  $g_i$ , is:

$$g_i \left( H_i^{n+1}, H_i^n, H_j^{n+1}, H_j^n \right) = \sum_{j \neq i, j \in \eta_i} \left( A_{ij}^{n+1} \left( H_j^{n+1} - H_i^{n+1} \right) \right) + \frac{1}{\Delta t^{n+1}} \sum_{j \in \sigma_i} \left( B_{ij} \left( \theta_j^{n+1} - \theta_j^n \right) \right) - F_i^{n+1} = 0 \quad (4)$$

where  $\eta_i$  includes node  $i$  and the set of its neighboring nodes; and  $\sigma_i$  represents the (set of) element(s) sharing node  $i$ . The expressions for matrices  $[A_{ij}]$  and  $[B_{ij}]$  for different formulations of FE and MHFE methods can be found in literature (e.g., Huyakorn et al., 1984; Chavent and Roberts, 1991; Belfort et al., 2009). It should be noted that for the FD/FV methods, the previous matrices are given by Eqs. (5) and (6):

$$A_{ij} = K_s \cdot K_{r,ij} \cdot \gamma_{ij} \quad (5)$$

where  $K_{r,ij}$  is the conductivity between cells  $i$  and  $j$ ; and  $\gamma_{ij}$  refers to the interface area between  $i$  and  $j$  divided by the distance between them.

$$B_{ij}^e = |V_e| \delta_{ij} \quad (6)$$

where  $|V_e|$  is the length (1D)/surface (2D)/volume (3D) of element “ $e$ ”; and  $\delta_{ij}$  is the Kronecker operator. The previous definition must be modified in the case of non-orthogonal control volumes (Loudy et al., 2007).

**Table 1**  
Effective saturation function and relative conductivity function.

References	Formulation and condition	Parameters
Brooks–Corey (1964) (BCM)	$Se = 1/(\alpha h )^{\lambda}$ $K_r = Se^{L+2+2/\lambda} \quad \alpha h < -1$	$\alpha$ : inverse of the air-entry value $\lambda$ : pore size index $L$ : pore connectivity parameter ( $L = 0.5$ following Mualem, 1976) ( $L = 1$ following Burdine, 1953)
Haverkamp et al. (1977) (HM)	$Se = B/(B +  h ^{\beta})$ $K_r = A/(A +  h ^{\alpha}) \quad h < 0$	A, B, $\alpha$ and $\beta$ : empirical parameters
van Genuchten (1980) (vGM)	$Se = 1/[1 + (\alpha h )^n]^m$ $K_r = Se^L [1 - (1 - Se^{1/m})^m]^2 \quad h < 0$	$m = 1 - 1/n$ (traditionally) $n$ and $\alpha$ : empirical constants $L$ : pore connectivity parameter ( $L = 0.5$ following Mualem, 1976) ( $L = 1$ following Burdine, 1953)
Gardner (1958), Russo (1988) (GRM)	$Se = e^{(-0.5 \times \alpha h )} \times [1 + 0.5 \times \alpha h ]^{2/m^2}$ $K_r = e^{(-\alpha h )} \quad h < 0$	$\alpha$ : pore size distribution parameter $m$ : form parameter (tortuosity)
Srivastava and Yeh (1991) (ExpM)	$Se = e^{(-\alpha h )}$ $K_r = e^{(-\alpha h )} \quad h < 0$	$\alpha$ : pore size distribution parameter
Fuentes et al. (1992) (vGBCM)	$Se = 1/[1 + (\alpha h )^n]^m$ $K_r = Se^L \quad h < 0$	$m = 1 - 2/n$ $\alpha$ and $L$ : empirical parameters
Modified van Genuchten Vogel et al. (2001) and Ippisch et al. (2006) (mvGM)	$S_e = 1/\{S_e^* [1 + (\alpha h )^n]^m\}$ $K_r = S_e^L \left[ \frac{1 - (1 - (S_e^*)^{1/m})^m}{1 - (S_e^*)^{1/m}} \right]^2 \quad h < -h_e$	$S_e^* = 1/[1 + (\alpha h_e)^n]^m$ $h_e$ : equivalent of the air entry value

When the pressure head condition is not satisfied,  $Se = 1$  and  $K_r = 1$

3.2. Monotonicity conditions

The monotonicity analysis is typically performed by considering the general form of the discretized RE (Eq. (4)). Following Forsyth and Kropinski (1997), it is established that a monotone discretization does not contain any local minima or maxima for all its interior homogeneous nodes:

$$H_i^{\min} \leq H_i^{n+1} \leq H_i^{\max} \tag{7}$$

where  $H_i^{\min} = \min(H_j^{n+1}, H_i^n)$  and  $H_i^{\max} = \max(H_j^{n+1}, H_i^n)$  ( $\forall j \in \eta_i$ ).

The monotonicity analysis can be achieved on the discretized (but not linearized) system of Eq. (4), which is equivalent to the opposing expression of Forsyth and Kropinski (1997). According to these authors, a monotone solution is required to satisfy the following conditions for all interior nodes:

$$(a^{\circ}) \frac{\partial g_i}{\partial H_i^n} \leq 0 \text{ and } (b^{\circ}) \frac{\partial g_i}{\partial H_j^{n+1}} \leq 0 \text{ and } (c^{\circ}) \frac{\partial g_i}{\partial H_i^{n+1}} > 0 \tag{8}$$

The different derivatives are given as follows:

$$\frac{\partial g_i}{\partial H_i^n} = -\frac{1}{\Delta t^{n+1}} B_{ii} \frac{\partial \theta_i^n}{\partial H_i^n} \tag{9}$$

$$\frac{\partial g_i}{\partial H_j^{n+1}} = \sum_{j \neq i, j \in \eta_i} \left( \frac{\partial A_{ij}^{n+1}}{\partial H_j^{n+1}} (H_j^{n+1} - H_i^{n+1}) \right) + A_{ij}^{n+1} + \frac{1}{\Delta t^{n+1}} B_{ij} \frac{\partial \theta_j^{n+1}}{\partial H_j^{n+1}} \tag{10}$$

$$\begin{aligned} \frac{\partial g_i}{\partial H_i^{n+1}} &= \sum_{j \neq i, j \in \eta_i} \left( \frac{\partial A_{ij}^{n+1}}{\partial H_i^{n+1}} (H_j^{n+1} - H_i^{n+1}) - A_{ij}^{n+1} \right) + \frac{1}{\Delta t^{n+1}} B_{ii} \frac{\partial \theta_i^{n+1}}{\partial H_i^{n+1}} - \frac{\partial F_i^{n+1}}{\partial H_i^{n+1}} \\ &= \sum_{j \neq i, j \in \eta_i} \left( \frac{\partial A_{ij}^{n+1}}{\partial H_i^{n+1}} (H_j^{n+1} - H_i^{n+1}) \right) + A_{ii}^{n+1} + \frac{1}{\Delta t^{n+1}} B_{ii} \frac{\partial \theta_i^{n+1}}{\partial H_i^{n+1}} - \frac{\partial F_i^{n+1}}{\partial H_i^{n+1}} \end{aligned} \tag{11}$$

3.3. Analysis of methods to ensure monotonicity

3.3.1. The issue of equivalent conductivity to avoid unphysical oscillations

Despite the fact that FV and FD schemes satisfy the M-Matrix property by definition (Forsyth and Kropinski, 1997), it was shown that FD numerical solutions might exhibit unphysical oscillations (Forsyth and Kropinski, 1997; Baker, 2006; Szymkiewicz, 2009). Furthermore, in the case of unsaturated flow and condition (b) of Eq. (8), the derivatives of the matrix [A] have to be considered, yielding a condition dependent on the estimation of the conductivity.

Interblock conductivity can be achieved using arithmetic, harmonic, geometric or more complex means of the hydraulic conductivities at the two adjacent cells (Haverkamp and Vauclin, 1979; Schnabel and Richie, 1984; Zaidel and Russo, 1992; Forsyth et al., 1995; Romano et al., 1998; van Dam and Feddes, 2000; Gastó

et al., 2002; Brunone et al., 2003). Table 2 summarizes the main formulations of equivalent/interblock conductivity that have been studied particularly for 1D flow problems. For the weighted mean proposed by Gastó et al. (2002) a critical size ( $\Delta z \leq [\alpha \cdot (a_{10} + a_{11} - \log(N))]^{-1}$ ) should be considered to avoid negative values of the conductivity, as is reported, for instance, by Szymkiewicz (2009) for large internodal spaces. Additionally, it should be observed that this weighted mean can be applied only for the van Genuchten (1980) and Brooks and Corey (1964) hydraulic models. Darcian mean approximations are preferred to avoid unphysical oscillations (Warrick, 1991; Baker, 1995; Baker et al., 1999; Baker, 2000, 2006). Table 3 provides the main formulas to compute the Darcian integral mean for the different hydraulic models. An adaptation is proposed to handle the classical formulation of the van Genuchten model rather than the simplified form used by Baker (2000). The weighting coefficients  $w_{GASTO}$  (Gastó et al., 2002) and  $\lambda_{DARC}$  (see Table 3) are functions of the conductivity at the two neighboring nodes. Notice that their expressions are not symmetric. In addition, previous studies (Baker et al., 1999; Baker, 2000, 2006) have shown interest in changing the expression of the equivalent conductivity (referred in Table 2 as  $K_{Optim}$ ) in function of the ratio  $\Delta h/\Delta z$ . Due to the complex computation of  $K_{darcy}$ , an alternative optimized algorithm has been recently developed to avoid oscillations (Szymkiewicz, 2009). The algorithm has been reproduced and slightly adapted to take into account the orientation of the vertical axis (see Appendice).

The purpose of the following paragraph is to complete the analysis proposed by Forsyth and Kropinski (1997), which showed that

the centroidal approximation is conditionally stable and suggests the use of upstream mean. For FD/FV methods and FE and MHFE variational formulations based on a single point quadrature rule, the relative hydraulic conductivity between nodes  $i$  and  $j$ , noted  $K_{r,eq}$ , should be estimated according to the possible expressions of Table 2. Hence, the expressions are obtained as follows:

$$\frac{\partial g_i}{\partial H_i^{n+1}} = \gamma_{ij} K_s \frac{\partial K_{r,eq}}{\partial H_j^{n+1}} (H_j^{n+1} - H_i^{n+1}) + A_{ij}^{n+1} + \frac{1}{\Delta t^{n+1}} B_{ij} \frac{\partial \theta_j^{n+1}}{\partial H_j^{n+1}} \quad (12)$$

$$\frac{\partial g_i}{\partial H_i^{n+1}} = \sum_{j \neq i, j \in \Omega_i} \left( \gamma_{ij} K_s \frac{\partial K_{r,eq}}{\partial H_i^{n+1}} (H_j^{n+1} - H_i^{n+1}) - A_{ij}^{n+1} \right) + \frac{1}{\Delta t^{n+1}} B_{ii} \frac{\partial \theta_i^{n+1}}{\partial H_i^{n+1}} \quad (13)$$

According to Eqs. (12) and (13), the results of the monotonicity analysis may depend on the relative conductivity estimation. Table 4 contains the analytical developments of the spatial terms of Eq. (12) for different equivalent conductivity estimations, and Table 5 summarizes the results related to Eq. (13). Regardless of the model chosen in Table 1 to describe the relationships between the pressure head and the relative conductivity,  $K_r(h)$  is an increasing function; therefore, the sign of its derivative remains positive. The sign of the expressions depicted in Tables 4 and 5 is important to determine if conditions (b) and (c) of Eq. (8) are satisfied. On one hand, we remark that the M-matrix criterion applied for the parameter  $\gamma_{ij}$  is a necessary but not always sufficient condition. On the other hand, the monotonicity of the different formulations should be studied specifically as follows:

**Table 2**

Formulations for the estimation of equivalent interblock conductivity for 1D discretizations, for FD/FV schemes or for FE/MHFE methods based on single point quadrature rule.

Formulation	Expression	References – comments
Arithmetic mean	$K_{arit} = 0.5[K_i + K_{i+1}]$	(e.g., Celia et al., 1990; van Dam and Feddes, 2000)
Geometric mean	$K_{geom} = [K_i + K_{i+1}]^{0.5}$	(e.g., Haverkamp and Vauclin, 1979)
Harmonic mean	$K_{harm} = 2[K_i^{-1} + K_{i+1}^{-1}]^{-1}$	(e.g., Oldenburg and Pruess, 1993; Romano et al., 1998; Manzini and Ferraris, 2004; Brunone et al., 2003) → especially for heterogeneous domain
Weighted mean	$K_{gasto} = w \cdot K_{upper} + (1 - w) \cdot K_{lower}$	(e.g., Warrick, 1991; Gastó et al., 2002) $K_{upper}$ ( $K_{lower}$ ) is the conductivity of the upper (lower) node
Upstream mean	$K_{up} = \begin{cases} K_i & \text{if } H_i \geq H_{i+1} \\ K_{i+1} & \text{if } H_i < H_{i+1} \end{cases}$	(e.g., Fuentes et al., 1992; Oldenburg and Pruess, 1993)
Integral mean	$K_{int} = \begin{cases} [h_{i+1} - h_i]^{-1} \cdot \int_{h_i}^{h_{i+1}} K(h) \cdot dh & \text{if } h_i \neq h_{i+1} \\ K_i & \text{if } h_i = h_{i+1} \end{cases}$	(e.g., Schnabel and Richie, 1984; Warrick, 1991; Zaidel and Russo, 1992)
Darcian integral mean	$K_{darcy} = \lambda_{darcy} \cdot K_{upper} + (1 - \lambda_{darcy}) \cdot K_{INT}$	(e.g., Baker, 1995; Baker et al., 1999; Baker, 2000); $K_{upper}$ is the conductivity of the upper node
Optimized algorithm	principle $\begin{cases} K_{INT} & \text{if } \frac{\Delta h}{\Delta z} \rightarrow \pm\infty \\ K_{UP} & \text{if } \frac{\Delta h}{\Delta z} \rightarrow 0 \text{ or } \frac{\Delta h}{\Delta z} \rightarrow \chi \end{cases}$	(Baker, 2006; Szymkiewicz, 2009) see Appendix → $\chi$ the cosine of the angle between the z axis and the direction of the gravity force

**Table 3**

Expression of the weighting coefficient for the Darcian integral mean approximation.

	$K_{darcy} = \lambda_{darcy} \cdot K_2 + (1 - \lambda_{darcy}) \cdot K_{int} \text{ (node 2 corresponds to the upper node)}$ $\lambda_{darcy} = \frac{(1 - e^{-u}) \Delta K (u - r_k) + (K_1 e^{-u} - K_2) r_k u}{(1 - e^{-u})[(\Delta K - K_2 r_k)u - \Delta K r_k + K_2 r_k^2]}$ <p>(see fortran code with all anticipated special conditions in Baker (2000))</p> $\Delta K = K_1 - K_2$ $r_k = \ln(K_1/K_2)$ $u = \frac{d}{K_r} \frac{\partial K_r}{\partial h}  _{heq} \text{ with } d = \text{distance between two adjacent nodes: (i) and (j) for instance}$
	$h_{eq} \rightarrow K_r(h_{eq}) = \sqrt{K_1 \cdot K_2} \text{ (for HM and BCM)}$ $h_{eq} \rightarrow \frac{K_r(h_{eq})}{Se^L(h_{eq})} = \sqrt{\frac{K_1}{Se_1^L} \frac{K_2}{Se_2^L}} \text{ (for vGM)}$
BCM	$u = \frac{n(L+2+\frac{2}{n})d}{ h_{eq} } = \frac{\alpha}{m} \cdot d \cdot (K_1 K_2)^{-m/2}, \quad m = -[n \times (L + 2 + \frac{2}{n})]^{-1}$ <p>and <math>K_{int} = \frac{m}{m+1} \frac{K_1^{m+1} - K_2^{m+1}}{K_2^m - K_1^m}</math></p>
HM	$u = \frac{d \cdot \alpha \cdot  h_{eq} ^{n-1}}{A k(h_{eq})} \approx d \cdot \alpha \cdot \frac{\Delta^{(-1/\alpha)}}{\sqrt{k_1 k_2}} \cdot \left[ \frac{1}{\sqrt{k_1 k_2}} - 1 \right]^{(1-\frac{1}{\alpha})}$ <p>and <math>K_{int}</math> by numerical integration</p>
vGM	$u \approx d \cdot \alpha \cdot L \cdot (n-1) \cdot (\alpha  h_{eq} )^{n-1} \cdot Se^{1/m} \cdot \left[ 1 + \frac{2 Se^{3/m} (1 - Se^{1/m})^{m-1}}{L \left[ \frac{k_1 k_2}{Se_1 Se_2} \right]^{1/4}} \right]$ <p>and <math>K_{int}</math> by numerical integration</p> $ h_{eq}  = \frac{1}{2} \left[ \left( 1 - \left( 1 - \left( \frac{k_1 k_2}{Se_1 Se_2} \right)^{\frac{1}{4}} \right)^{\frac{1}{m}} \right) - 1 \right]^{\frac{1}{\alpha}}$
vGBCM	$u \approx d \cdot L \cdot (n-2) \cdot \frac{(\alpha  h_{eq} )^n}{ h_{eq} (1 + (\alpha  h_{eq} )^n)}$ <p>and <math>K_{int}</math> by numerical integration</p> $ h_{eq}  = \frac{1}{2} [(k_{r1} k_{r2})^{-1/2Lm} - 1]^{\frac{1}{\alpha}}$
GRM and ExpM	$u = \alpha \cdot d \text{ and } K_{int} = \frac{K_1 - K_2}{\ln(K_1/K_2)}$

- The analytical expressions corresponding to the arithmetic, geometric, harmonic and weighted formulations show that the monotonicity depends on the piezometric variation between adjacent nodes weighted by a coefficient dependent on the relative conductivity and its derivative. A criterion that may guarantee the solution's monotonicity in the general case cannot be proposed.
- For the upstream mean, if the M-matrix criterion is satisfied, conditions (b) and (c) of Eq. (8) are automatically fulfilled, as can be seen in Tables 4 and 5. Despite this interesting property, the upstream formulation is sometimes avoided because of its overestimation of infiltration front.
- Assuming that the M-matrix criterion is satisfied and considering the expressions provided in Tables 4 and 5 for the integral mean, one can deduce that monotonicity is always accounted for horizontal flow processes. This fact corroborates the experimental conclusion of Pei et al. (2012). For vertical discretizations, a limitation has to be added. When the pressure gradient increases, i.e., the term  $\frac{\Delta h_{ji}}{\Delta z_{ji}} \rightarrow \pm\infty$ , Tables 4 and 5 show that the monotonicity conditions are reduced to the M-matrix condition. However, when the pressure gradient decreases, monotonicity difficulties appear to satisfy condition (c) of Eq. (8) if  $\frac{|\Delta h_{ji}|}{\Delta z_{ji}} \rightarrow 0^+$  and condition (b) if  $\frac{|\Delta h_{ji}|}{\Delta z_{ji}} \rightarrow 0^-$ . It should be noted that the expressions of Tables 4 and 5 could be modified if the z axis is not collinear to the gravity force by an angle  $\varphi$ . In this case, conditions (b) and (c) of Eq. (8) can be written as follows:

$$(K_{r,int} - K_{r,i}) \left( \frac{\Delta z_{ji}}{\Delta h_{ji}} \chi \right) - K_{r,i} \leq 0 \tag{14}$$

$$(K_{r,j} - K_{r,int}) \left( \frac{\Delta z_{ji}}{\Delta h_{ji}} \chi \right) + K_{r,j} > 0 \tag{15}$$

with  $\chi = \cos(\varphi)$ . Because  $K_{r,int}$  is between  $K_{r,i}$  and  $K_{r,j}$ , when  $\frac{\Delta h}{\Delta z} \rightarrow \chi$ , Eqs. (14) and (15) lead to conditions (16) that can never be satisfied and are given as follows:

$$K_{r,int} \leq 2K_{r,i} \text{ and } K_{r,int} < 2K_{r,j} \tag{16}$$

Hence, our mathematical analysis demonstrates that the integral formulation could produce unphysical oscillations. The analysis corroborates previous studies of the flux approximation based on a simple three-point grid (Baker, 2000, 2006; Szymkiewicz, 2009).

- The monotonicity of the optimized algorithm (Szymkiewicz, 2009) is more difficult to attest. Hence, we provide in appendix an analytical analysis of monotonicity based on Eq. (8). The main result is that the formulation used to estimate internodal conductivity during infiltration is unconditionally stable. For drainage, monotonicity has been demonstrated for the expression  $K_1$  based on the upper conductivity (see Eq. (A.2) in Appendix). The heuristic formulation used for  $K_2$  is conditionally monotonic. It should be noticed that the presence of relative conductivity derivatives in the final expressions prevents any general conclusions. Nonetheless, as stated by Szymkiewicz (2009), oscillations in drainage problem are linked with overestimation of internodal conductivity. Since the minimum value of  $(K_1, K_2)$  is chosen, monotonicity should be preserve. The complex heuristic formulation of  $K_{eq}$  used for capillary rise does not allow us to conclude easily on monotonicity accordingly to the criterion of Eq. (8).

### 3.3.2. Propositions of algorithm

To simplify the presentation, we suppose that the multidimensional existing code uses a centroidal approximation for the evaluation of the equivalent conductivity. Centroidal approximation signifies that the conductivity over each element is computed from a combination of the conductivities at the nodal points (edges/faces). The arithmetic mean (e.g., Šimůnek et al., 2006) appears as a particular and, nonetheless, currently used technique. Hence, Eq. (10) is modified to hold this specific context:

$$\frac{\partial g_i}{\partial H_j^{n+1}} = K_s \frac{\partial (K_{r,eq}^{n+1})_{E_{ij}}}{\partial H_j^{n+1}} \sum_{\ell \neq i, \ell \in \eta_i} (\gamma_{i\ell} (H_\ell^{n+1} - H_i^{n+1})) + \gamma_{ij} K_s (K_{r,eq}^{n+1})_{E_{ij}} \tag{17}$$

**Table 4**  
Development of the two right hand side terms of Eq. (12).

$K_{r,eq}$ Formulation	$\gamma_{ij} \frac{\partial K_{r,eq}}{\partial h_j^{n+1}} (H_j^{n+1} - H_i^{n+1}) + A_{ij}$
Arithmetic mean	$\frac{1}{2} \gamma_{ij} \left[ \frac{\partial K_{r,j}}{\partial h_j^{n+1}} (H_j^{n+1} - H_i^{n+1}) + (K_{r,i} + K_{r,j}) \right]$
Geometric mean	$\gamma_{ij} \sqrt{K_{r,i} K_{r,j}} \left[ \frac{K_{r,i}}{2(K_{r,i} K_{r,j})} \frac{\partial K_{r,j}}{\partial h_j^{n+1}} (H_j^{n+1} - H_i^{n+1}) + 1 \right]$
Harmonic mean	$2\gamma_{ij} (K_{r,i}^{-1} + K_{r,j}^{-1})^{-1} \left[ (K_{r,i}^{-1} + K_{r,j}^{-1})^{-1} K_{r,j}^2 \frac{\partial K_{r,j}}{\partial h_j^{n+1}} (H_j^{n+1} - H_i^{n+1}) + 1 \right]$
Weighted mean	$\gamma_{ij} \left[ ((1-w) \frac{\partial K_{r,j}}{\partial h_j^{n+1}} + (K_{r,i} - K_{r,j}) \frac{\partial w}{\partial h_j^{n+1}}) (H_j^{n+1} - H_i^{n+1}) + (wK_{r,i} + (1-w)K_{r,j}) \right]$
Upstream mean	$\begin{cases} \gamma_{ij} K_{r,j} & \text{if } H_i^{n+1} > H_j^{n+1} \\ \gamma_{ij} \left[ \frac{\partial K_{r,j}}{\partial h_j^{n+1}} (H_j^{n+1} - H_i^{n+1}) + K_{r,j} \right] & \text{if } H_i^{n+1} \leq H_j^{n+1} \end{cases}$
Integral mean	$\begin{cases} \gamma_{ij} \left[ (K_{r,j} - K_{r,int}) \left( \frac{z_j - z_i}{h_j - h_i} \right) + K_{r,j} \right] & \text{if } h_i \neq h_j \\ \gamma_{ij} \left[ \frac{\partial K_{r,j}}{\partial h_j^{n+1}} (z_j - z_i) + K_{r,j} \right] & \text{if } h_i = h_j \end{cases}$
Darcian integral mean	If “i” is the upper node $\gamma_{ij} \left\{ \left[ (K_{r,i} - K_{r,int}) \frac{\partial z}{\partial h_j^{n+1}} + (1-\lambda) \frac{\partial K_{r,int}}{\partial h_j^{n+1}} \right] (H_j^{n+1} - H_i^{n+1}) + (\lambda K_{r,i} + (1-\lambda) K_{r,int}) \right\}$
Optimized algorithm	If “j” is the upper node $\gamma_{ij} \left\{ \left[ (K_{r,j} - K_{r,int}) \frac{\partial z}{\partial h_j^{n+1}} + \lambda \frac{\partial K_{r,j}}{\partial h_j^{n+1}} + (1-\lambda) \frac{\partial K_{r,int}}{\partial h_j^{n+1}} \right] (H_j^{n+1} - H_i^{n+1}) + (\lambda K_{r,i} + (1-\lambda) K_{r,int}) \right\}$ See Appendix

where  $E_{ij}$  refers to the element containing nodes  $i$  and  $j$ ;  $(K_{r,eq}^{n+1})_{E_{ij}}$  is the average conductivity over this element, and  $\eta_i$  includes node  $i$  and the set of its neighboring nodes. To obtain a monotonic solution of the RE, we investigate two strategies presented in the following paragraphs.

For all the interior and homogeneous nodes of the domain, the monotonicity of the solution is tested at each time step.

With the first strategy (MS1), a subroutine tests the monotonicity of the solution at each time step. When unphysical oscillations are encountered, MS1 consists of stopping the iterative process, imposing the upstream formulation (either at specific nodes or at all nodes) and running the numerical code again for the problematic time step. Then, the equivalent conductivity retrieves its original formulation until oscillations reappear. The MS1 algorithm only considers the elements without sink/source term and whose neighbors are constituted of the same soil material.

In the second approach (MS2), the value of the equivalent conductivity is adapted in function of condition (b) of Eq. (8). Therefore, the algorithm is based on the following test:

$$\forall i \text{ and } j \in \eta_i^E, i \neq j \quad \gamma_{ij} K_s (K_{r,eq}^{n+1,k})_{E_{ij}} + K_s \frac{\partial (K_{r,eq}^{n+1,k})_{E_{ij}}}{\partial h_j^{n+1,k}} \sum_{\ell \neq i, \ell \in \eta_i^E} (\gamma_{i\ell} (H_i^{n+1,k} - H_\ell^{n+1,k})) \leq 0 \quad (18)$$

where  $\eta_i^E$  refers to node  $i$  and the set of its neighboring nodes belonging to element  $E$ . During the iterative process, either the equivalent conductivity satisfies Eq. (18) or the upstream approximation, which guaranties the monotonicity, is substituted. In fact, for a  $N_E$  nodes

element, Eq. (18) represents a system of  $N_E \times (N_E - 1)$  equations. It should be noted that the coefficients  $\gamma_{ij}$  depend only on the mesh geometry and have been already computed for solving the matrix system corresponding to Eq. (3). Only the derivative of  $K_{r,eq}^{n+1}$ , i.e., especially the derivative of the  $K(h)$  function, could necessitate additional work. When the Newton–Raphson iteration is used, a subroutine is typically implemented for the analytical evaluation of these derivatives, which is required for the Jacobian matrix computation.

It should be noted that for different simulations, numerical codes based on the mass-lumped MHFE method have been used.

#### 4. Numerical simulations

The purpose of this section is to illustrate the theoretical monotonicity assessments by computing the expressions of Table 4 for different types of soil, mesh sizes and constitutive relationships and investigate unsteady flow simulations showing the effect of the equivalent conductivity and efficiency of the proposed algorithm. The relative conductivity, water content and capillary capacity are computed directly from the definitions provided in Table 1. For the hydraulic models of van Genuchten (1980), Haverkamp et al. (1977) and Fuentes et al. (1992), the integral formulation of the equivalent conductivity is estimated with a Gauss-Legendre numerical integration, whereas for the Brooks–Corey and the exponential models, the analytical expressions have been implemented. In addition, the derivatives in Table 4 are determined analytically, except for the derivatives of the weighting coefficient occurring in the weighted ( $w_{GASTO}$ ) and Darcian integral means ( $\lambda_{DARC}$ ), which are estimated with a perturbation method. For the weighted

**Table 5**  
Development of the first right hand side term of Eq. (13).

$K_{r,eq}$ Formulation	$\gamma_{ij} \frac{\partial K_{r,eq}}{\partial h_j^{n+1}} (H_j^{n+1} - H_i^{n+1}) + A_{ij}$
Arithmetic mean	$\frac{1}{2} \gamma_{ij} \left[ \frac{\partial K_{r,j}}{\partial h_j^{n+1}} (H_j^{n+1} - H_i^{n+1}) + (K_{r,i} + K_{r,j}) \right]$
Geometric mean	$\gamma_{ij} \sqrt{K_{r,i} K_{r,j}} \left[ \frac{K_{r,i}}{2(K_{r,i} K_{r,j})} \frac{\partial K_{r,j}}{\partial h_j^{n+1}} (H_j^{n+1} - H_i^{n+1}) - 1 \right]$
Harmonic mean	$2\gamma_{ij} (K_{r,i}^{-1} + K_{r,j}^{-1})^{-1} \left[ (K_{r,i}^{-1} + K_{r,j}^{-1})^{-1} K_{r,j}^{-2} \frac{\partial K_{r,i}}{\partial h_i^{n+1}} (H_i^{n+1} - H_j^{n+1}) - 1 \right]$
Weighted mean	$\gamma_{ij} \left[ \left( \frac{\partial K_{r,i}}{\partial h_i^{n+1}} + (K_{r,i} - K_{r,j}) \frac{\partial w}{\partial h_i^{n+1}} \right) (H_i^{n+1} - H_j^{n+1}) - (wK_{r,i} + (1-w)K_{r,j}) \right]$
Upstream mean	$\begin{cases} \gamma_{ij} \left[ \frac{\partial K_{r,i}}{\partial h_j^{n+1}} (H_j^{n+1} - H_i^{n+1}) + K_{r,j} \right] & \text{if } H_i^{n+1} > H_j^{n+1} \\ -\gamma_{ij} K_{r,j} & \text{if } H_i^{n+1} \leq H_j^{n+1} \end{cases}$
Integral mean	$\begin{cases} \gamma_{ij} \left[ (K_{r,i} - K_{r,int}) \left( \frac{z_j - z_i}{h_j - h_i} \right) + K_{r,i} \right] & \text{if } h_i \neq h_j \\ \gamma_{ij} \left[ \frac{\partial K_{r,i}}{\partial h_i^{n+1}} (z_j - z_i) + K_{r,i} \right] & \text{if } h_i = h_j \end{cases}$
Darcian integral mean	If “i” is the upper node $\gamma_{ij} \left\{ \left[ \lambda \frac{\partial K_{r,i}}{\partial h_i^{n+1}} + (1-\lambda) \frac{\partial K_{r,int}}{\partial h_i^{n+1}} + (K_{r,i} - K_{r,int}) \frac{\partial z}{\partial h_i^{n+1}} \right] (H_j^{n+1} - H_i^{n+1}) - (\lambda K_{r,i} + (1-\lambda) K_{r,int}) \right\}$
	If “j” is the upper node $\gamma_{ij} \left\{ \left[ (1-\lambda) \frac{\partial K_{r,int}}{\partial h_i^{n+1}} + (K_{r,j} - K_{r,int}) \frac{\partial z}{\partial h_i^{n+1}} \right] (H_j^{n+1} - H_i^{n+1}) - (\lambda K_{r,j} + (1-\lambda) K_{r,int}) \right\}$
Optimized algorithm	See Appendix

formulation of Gastó et al. (2002), when the mesh size increases, the weighting coefficient can be negative. In this case, the upstream mean can substituted to avoid numerical problems.

#### 4.1. Accuracy assessment for steady state flow

In this section, the expressions of Table 4 are computed without considering the coefficient  $\gamma_{ij}$ , which depends on the numerical scheme and mesh geometry. Due to the summation term and presence of mass variation for diagonal coefficients (see Eq. (13)), the expressions depicted in Table 5 are not computed. Sixteen types of soils covering different texture classes presented by Szymkiewicz (2009) have been selected. Five hydraulic models depicted in Table 1 are used and the corresponding parameters are reported in Table 6. We consider  $25 \times 10^4$  possible values for the pressure variation  $(h_j - h_i)$ , and the nodal distance  $d_{ij}$  takes the values of  $\pm 1$  cm,  $\pm 10$  cm,  $\pm 100$  cm or  $\pm 200$  cm along the vertical direction. As shown in Fig. 1, our numerical approach allows testing the monotonicity of the different equivalent conductivity formulations for various scenarios corresponding to infiltration, drainage or capillary rise. The behavior of the different means has been largely described in literature (Szymkiewicz, 2009) by comparing the accuracy of each formulation when the nodal spacing increases.

The results of these numerous simulations for vertical flow are summarized in Fig. 2. For each type of soil and nodal distance, we report the percentage of positive value for the coefficients of Eq. (12). As expected, the upstream mean always leads to positive values for the coefficient of Eq. (12), and consequently, its results are not shown on Fig. 2. Below a critical mesh size, the weighted formulation of Gastó et al. (2002) has an approximately monotonic behavior. The geometric, harmonic and integrated means appear to be extremely

sensitive to oscillation problems, especially for large grid size and coarse-textured soils. The Darcian integral mean is more interesting from this point of view. Contrary to the arithmetic mean, it remains stable when the mesh size increases. Finally, it is worth noting that Szymkiewicz’s algorithm produces monotonic solution for the different grid sizes and soils used for these steady state cases.

#### 4.2. Numerical simulations of time varying unsaturated flow

In the current section, we propose to analyze the efficiency of our monotonicity analysis by different test cases illustrating infiltration, drainage and evaporation processes for both one and two-dimensional problems. Both temporal and spatial unphysical oscillations are considered. For one-dimensional problems, a FD numerical code using the Thomas algorithm has been used to solve the mixed form of RE. The time step size management is achieved by using a heuristic method based on the number of iterations (Šimůnek et al., 2006). It should be noted that more advanced time integration methods (e.g., Miller et al., 1998) and/or time stepping techniques (Belfort et al., 2007) could be used to improve the efficiency of the model.

Besides, in this section, only some averaging techniques were selected either because of the performance obtained in the previous steady-state investigations and/or reported in literature ( $K_{szym}$ ) or because of their adaptability in multidimensionnels codes ( $K_{arit}$ ,  $K_{geom}$ ). Hence,  $K_{gasto}$ ,  $K_{int}$  and  $K_{darcy}$  were not considered.

Statistical results are provided in Table 7 to illustrate the monotonicity and efficiency of various averaging schemes and algorithms for 1D problems. Hence, the root mean square error,

$\theta - RMSE_{\Delta z} = \sqrt{\frac{1}{N_{\Delta z}} \sum_{i=1}^{N_{\Delta z}} (\theta_i - \theta_{ref,i})^2}$ , the potential head gradient and, the maximum pressure overshoot for infiltration have been

reported. Fine grid solutions ( $\Delta z$  between 1 and 0.5 mm) have been computed and serve as reference solutions ( $O_{ref}$ ) for error calculations. For two-dimensional problems, the new algorithm has been implemented in a lumped MHFE numerical code. The linear system is solved with the preconditioned conjugate gradient method, and the time step size is heuristically adapted.

4.2.1. Test problem 1: infiltration with constant head boundary condition in a 1D domain

The first test case is selected from Baker et al. (1999) and demonstrates the difficulties of arithmetic formulation to produce physically admissible results. This case deals with infiltration in a 45-m-deep column, which contains moderately to coarsely textured soils. The soil hydraulic properties are characterized by Haverkamp’s model (see Table 1), and the parameters are summarized in Table 6 (soil no = 13). The media is initially dry, and  $h(z, 0) = h_{mit} = -929.8$  cm. This pressure head is maintained at the bottom during the simulation,  $h(z = 450 \text{ cm}, t) = h_{down} = -929.8$  cm, and the top boundary condition is  $h(z = 0 \text{ cm}, t) = h_{top} = -20.7$  cm. For the time step management, we adopt a minimum value of  $10^{-3}$  s and maximum time step of 100 s. The simulation is performed over 1.5 days.

Fig. 3 describes the evolution of the water content at the position  $z = 1200$  cm for a uniform mesh size of 150 cm. During the infiltration process, this type of profile should be monotone; however, large oscillations are observed in Fig. 3. The temporal evolution of the matrix coefficient corresponding to the modified Picard iteration method and the coefficient of Eq. (12) are also presented in Fig. 3. When the oscillations occur, only the coefficient of Eq. (12) becomes positive. This result demonstrates the necessity to include the derivatives in the monotonicity analysis. Comparisons between the standard approach and MS1 or MS2 algorithms are shown in Fig. 4, which depicts the profiles of water content after 30 h of infiltration. On one hand, the arithmetic formulation exhibits large spatial oscillations when the grid size increases from 10 cm to 150 cm (Table 7), whereas the upstream approximation leads to an oscillation-free solution corresponding to a faster than expected wetting front. On the other hand, the Darcian mean approximation  $K_{szym}$  and the new algorithms associated with the arithmetic or geometric means produce physically admissible results. Statistical results presented in Table 7 show that many extremum appear with a standard approach based on  $K_{geom}$  or  $K_{arit}$ . These failures correspond mainly to pressure overshoots that have been reported in Table 7 for different grid sizes. Indeed we provide the maximum value of the potential head gradient (referred as  $\max(\Delta h/\Delta z)$  in Table 7); for a problem of infiltration, positive values indicate the presence of oscillation

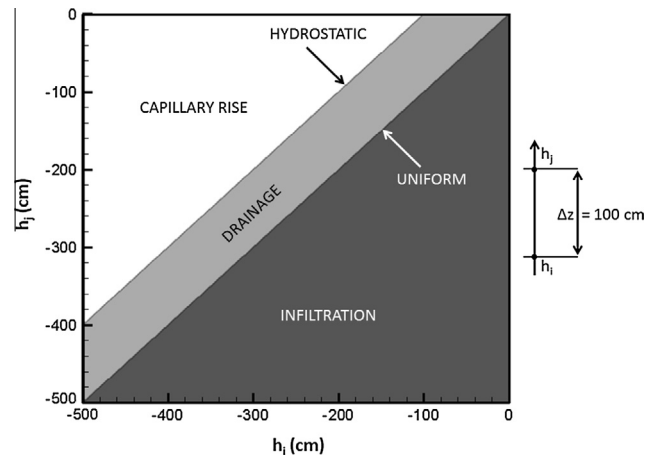


Fig. 1. Illustration of the various situations covered by the  $25 \times 10^4$  couples of values  $(h_i, h_j)$  for the grid size 100 cm.

in the solution. On the contrary,  $K_{szym}$  and  $K_{up}$  do not produce any oscillations and have not been combined with MS1 or MS2 algorithms. We can observe in Table 7 that  $K_{szym}$  improves the accuracy of the solution obtained with the upstream mean. Otherwise, the MS2 algorithm detects many violations of the monotonicity criterion that lead to a conductivity modification. The MS1 algorithm avoids both the presence of oscillation in the solution and its propagation in the profile. Stabilizing the solution at a given time is necessary but not sufficient, and MS1 has to correct the conductivity regularly during simulation. For this first test case of infiltration in dry soil, the new algorithms maintain the precision of the results achieved by the arithmetic formulation and avoid spurious oscillations as depicted in Table 7 and Fig. 4. The precision of the new algorithm (MS1) is slightly better than the optimized algorithm ( $K_{szym}$ ), mainly with the geometric mean.

Notice that the Newton–Raphson iterative method (Lehmann and Ackerer, 1998) and the Method of Lines (Miller et al., 1998) have been implemented and tested (results not shown). Even if these methods improve the convergence and rapidity of the computation, we can observe similar unphysical oscillations in the solutions.

4.2.2. Test problem 2: drainage in 1D sand column

The second test problem, which has been investigated by Szymkiewicz (2009), studies the effects of other flow conditions. A 5-m-deep sand column (soil no. 5) is considered with the following

Table 6  
Hydraulic parameters of the soils used for the monotonicity illustration.

Soil no.	Model	$\alpha$ (cm <sup>-1</sup> )	$n, \lambda$ ou $\beta$ (-)	$m$ ou $B$ (-)	$L$ ou $A$ (-)	$\theta_s$ (-)	$\theta_r$ (-)	$K_s$ (cm s <sup>-1</sup> )	Type	References
1	vGM	0.1449	2.68	0.627	0.5	0.430	0.045	$8.25 \times 10^{-3}$	Sand	Carsel and Parrish (1988)
2	vGM	0.0752	1.89	0.471	0.5	0.41	0.065	$1.23 \times 10^{-3}$	Sandy loam	
3	vGM	0.0200	1.41	0.291	0.5	0.45	0.067	$1.25 \times 10^{-4}$	Silty loam	
4	vGM	0.0050	1.09	0.083	0.5	0.38	0.068	$5.56 \times 10^{-5}$	Silty clay	
5	BCM	0.1389	0.592	-	0.5	0.430	0.045	$5.83 \times 10^{-3}$	Sand	Rawls et al. (1982)
6	BCM	0.0680	0.322	-	0.5	0.412	0.041	$7.19 \times 10^{-4}$	Sandy loam	
7	BCM	0.0483	0.211	-	0.5	0.486	0.015	$3.67 \times 10^{-4}$	Silty loam	
8	BCM	0.0292	0.127	-	0.5	0.423	0.056	$2.5 \times 10^{-5}$	Silty clay	
9	vGM	0.0260	2.23	0.552	-1.28				Sand	Schaap and Leij (2000)
10	vGM	0.0408	1.19	0.160	-6.97				Clay	
11	vGM	0.0249	1.507	0.336	-0.14	0.43	0.01	$2.03 \times 10^{-4}$	Sand	van Dam and Feddes (2000)
12	vGBCM	0.0331	7	0.714	7				Sand	Szymkiewicz et al. (2008)
13	vGBCM	0.1613	2.97	0.327	5.05				Chernobil soil	Lassabatere et al. (2006)
14	HM	4.7400	3.96	$1.611 \times 10^6$	$1.18 \times 10^6$	0.212	0.075	$9.44 \times 10^{-3}$		Haverkamp et al. (1977)
15	GRM	1.0000	-	-	-					
16	GRM	0.0100	-	-	-					

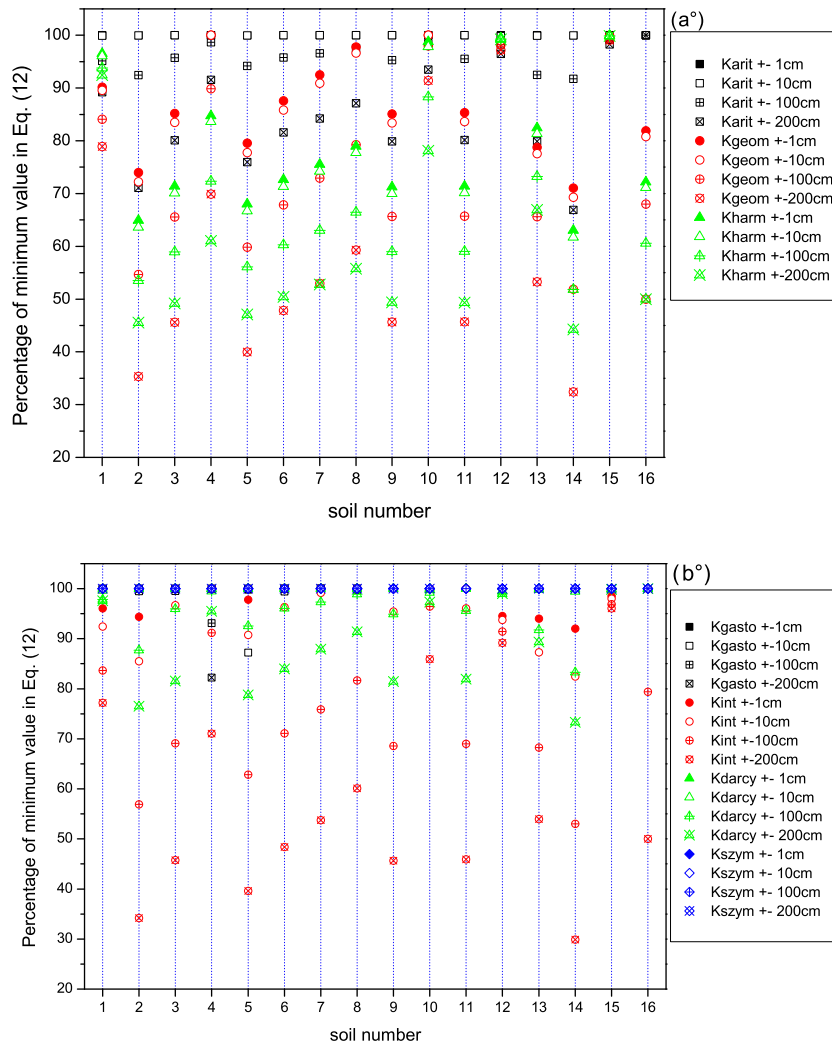


**Fig. 2.** Steady state tests: percentage of minimum value of the coefficient of Eq. (12) in vertical direction for different soils and mesh sizes (a°)  $K_{arit}$ ,  $K_{geom}$ ,  $K_{harm}$ ; (b°)  $K_{gasto}$ ,  $K_{int}$ ,  $K_{darcy}$ ,  $K_{szym}$ .

properties: the media is quasi-saturated with a uniform pressure head distribution,  $h(z, 0) = h_{init} = -7.5$  cm, the lower boundary pressure head remains at the same initial value while an impermeable boundary condition is imposed at the top of the column, and  $q(z = 0 \text{ cm}, t) = q_{top} = 0 \text{ cm s}^{-1}$ . The time step size varies automatically between  $3.6 \times 10^{-6}$  s and 360 s according to the number of iterations. The pressure head profiles after 30 h of drainage are illustrated in Fig. 5 which are similar to those presented by Szymkiewicz (2009). The simple averaging methods,  $K_{geom}$  and  $K_{arit}$ , produce large oscillations in the solution. The methods based on the Darcian mean produce oscillation-free solutions. The MS1 algorithm allows removal of the unphysical oscillations from the solutions obtained with the simple averaging techniques and conserves the trend of the chosen equivalent conductivity. Hence, the accuracy of the algorithm is good and for coarse grid slightly better than simple original formulations. As observed in Table 7, the monotonicity test is so restrictive that the MS2 approach uses many changes of the conductivity. Hence, the corresponding solutions are similar to  $K_{up}$  and have not been drawn. The monotonicity failures reported in Table 7 correspond to oscillations in the profile at a given time. Contrary to the first test case, these numerical artifacts do not produce overshoot of the maximum pressure head but the minimum value of the potential head gradient (referred as  $\min(\Delta h/\Delta z)$  in Table 7) should be positive or null. Postive values of this

gradient observed for  $K_{arit}$  and  $K_{geom}$  indicate spurious oscillations in the drainage process.

#### 4.2.3. Test problem 3: intensive rain at a 1D dry heterogeneous soil

This test case allows investigation of the behavior of the averaged conductivity in the presence of soil heterogeneities. Two equal adjacent zones are considered, which represent a 14-m-deep one-dimensional domain. A rainfall rate of 0.25 m/day is applied over 7.5 days to an initially dry porous media ( $h_{init} = -1000$  cm). The material properties correspond to a soil value of no. 1 in Table 6, except that the modified van Genuchten model is used with an air entry pressure of 2 cm. A simple heterogeneity has been generated by considering a saturated permeability of the lower zone that is 10 times less than the original prescribed value in Table 6. The time step can vary between  $1 \times 10^{-6}$  s and 100 s according to a heuristic management. In this test case, spurious oscillations occurring upstream of the permeability discontinuity are reported in a few profiles of saturation (Fig. 6). From a physical point of view, the relatively small contrast of permeability causes a natural increase in saturation in the middle of the domain. When the arithmetic average is selected, unphysical oscillations appear before the wetting front reaches the lower zone, as depicted in Fig. 6a. Fine grid solutions are depicted for the different observation times (4.5d, 6d and 7.5d). Local extrema occurring in the interior part

**Table 7**  
Statistical results for the 1D test cases.

Keq		Karit	Karit MS1	Karit MS2	Kgeom	Kgeom MS1	Kgeom MS2	Kszym	Kup	
TEST 1 (t = 36 h)	NTS <sub>150</sub>	1354	1347	1387	1642	1315	1354	1345	1350	
	NI <sub>150</sub>	9559	14,252	10,134	8818	10,286	10,475	7947	9461	
	NMF <sub>150</sub>	8039	1109	9621	10,085	994	10,474	0	0	
	$\theta$ -RMSE <sub>150</sub>	4.63E-03	5.04E-03	6.42E-03	4.99E-02	3.90E-02	1.41E-02	1.14E-02	1.41E-02	
	MPO <sub>150</sub>	2.58E+00	0.00E+00	0.00E+00	5.27E+02	0.00E+00	0.00E+00	0.00E+00	0.00E+00	
	max ( $\Delta h/\Delta z$ ) <sub>150</sub>	3.70E-02	0.00E+00	0.00E+00	8.70E-01	0.00E+00	0.00E+00	0.00E+00	0.00E+00	
	$\theta$ -RMSE <sub>100</sub>	4.57E-02	4.51E-02	4.64E-02	2.89E-02	3.25E-02	4.74E-02	4.69E-02	7.09E-02	
	MPO <sub>100</sub>	3.49E+00	0.00E+00	0.00E+00	3.24E+02	0.00E+00	0.00E+00	0.00E+00	0.00E+00	
	max ( $\Delta h/\Delta z$ ) <sub>100</sub>	5.52E-02	0.00E+00	0.00E+00	6.92E-01	0.00E+00	0.00E+00	0.00E+00	0.00E+00	
	$\theta$ -RMSE <sub>50</sub>	4.72E-02	4.70E-02	4.75E-02	4.33E-02	4.30E-02	4.80E-02	4.76E-02	4.81E-02	
	MPO <sub>50</sub>	5.83E-01	0.00E+00	0.00E+00	9.52E+01	0.00E+00	0.00E+00	0.00E+00	0.00E+00	
	max ( $\Delta h/\Delta z$ ) <sub>50</sub>	2.51E-02	0.00E+00	0.00E+00	5.33E-01	0.00E+00	0.00E+00	0.00E+00	0.00E+00	
	$\theta$ -RMSE <sub>10</sub>	4.76E-02	4.76E-02	4.76E-02	4.73E-02	4.73E-02	NC	4.75E-02	4.78E-02	
	MPO <sub>10</sub>	0.00E+00	0.00E+00	0.00E+00	3.42E+00	0.00E+00	NC	0.00E+00	0.00E+00	
max ( $\Delta h/\Delta z$ ) <sub>10</sub>	0.00E+00	0.00E+00	0.00E+00	2.74E+00	0.00E+00	NC	0.00E+00	0.00E+00		
TTEST 2 (t = 30 h)	NTS <sub>50</sub>	550	660	510	533	688	510	511	510	
	NI <sub>50</sub>	2427	5405	2255	2374	5446	2255	2270	2255	
	NMF <sub>50</sub>	2218	455	2254	1948	431	2254	0	0	
	$\theta$ -RMSE <sub>50</sub>	2.75E-02	6.43E-03	8.99E-03	2.33E-02	6.25E-03	8.99E-03	6.48E-03	8.99E-03	
	min ( $\Delta h/\Delta z$ ) <sub>50</sub>	-6.88E-01	2.10E-02	2.00E-02	-3.95E-01	4.30E-03	2.00E-02	1.53E-02	2.00E-02	
	$\theta$ -RMSE <sub>25</sub>	1.07E-02	2.70E-03	5.53E-03	7.14E-03	2.69E-03	5.49E-03	2.27E-03	5.64E-03	
	min ( $\Delta h/\Delta z$ ) <sub>25</sub>	-4.47E-01	1.68E-02	1.84E-02	-2.80E-01	1.45E-02	1.84E-02	1.45E-02	1.84E-02	
	$\theta$ -RMSE <sub>10</sub>	1.69E-03	1.73E-03	2.29E-03	9.24E-04	9.63E-04	9.27E-04	1.00E-03	2.86E-03	
	min ( $\Delta h/\Delta z$ ) <sub>10</sub>	0.00E+00	0.00E+00	0.00E+00	0.00E+00	0.00E+00	0.00E+00	0.00E+00	0.00E+00	
	$\theta$ -RMSE <sub>1</sub>	1.25E-05	1.25E-05	1.25E-05	1.49E-05	1.49E-05	1.49E-05	1.13E-04	3.17E-04	
	min ( $\Delta h/\Delta z$ ) <sub>1</sub>	0.00E+00	0.00E+00	0.00E+00	0.00E+00	0.00E+00	0.00E+00	0.00E+00	0.00E+00	
	TEST 3 (t = 7.5 d)	NTS	7104	6970	6970	NC	NC	6972	6954	6972
		NI	30,328	43,297	26,794	NC	NC	26,637	27,059	26,637
		NMF	46,969	4380	25,140	NC	NC	26,561	0	0
$\theta$ -RMSE <sub>50</sub>		4.14E-02	1.47E-02	1.17E-02	NC	NC	1.55E-02	1.19E-02	1.55E-02	
$\theta$ -RMSE <sub>25</sub>		2.14E-02	2.09E-02	2.36E-02	NC	NC	2.00E-02	1.98E-02	2.00E-02	
$\theta$ -RMSE <sub>10</sub>		1.44E-02	1.16E-02	9.17E-03	NC	NC	1.27E-02	1.07E-02	1.27E-02	

NTS (Number of time step); NI (Number of iteration); NMF (Number of monotonicity failure eventually before correction); NC (no convergence); MS1 (if local extremum, algorithm uses Kup for all the cells); MS2 (if the monotonicity test is not verified, the algorithm uses Kup for all the cells);  $\theta$ -RMSE<sub>x</sub> (root mean square error on water content for a grid size of x cm); MPO<sub>x</sub> (maximum pressure overshoot for a grid size of x cm).

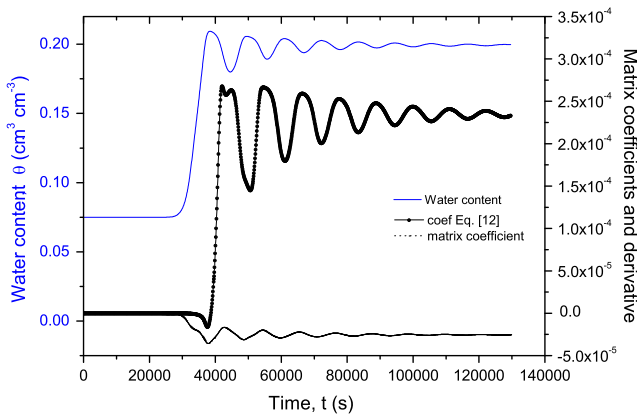


**Fig. 3.** Test case 1: evolution of the water content, the matrix coefficient and the coefficient of Eq. (12) at the location z = 1.2 m for the arithmetic mean.

of the upper zone decrease by reducing the nodal spacing. Otherwise, numerical oscillations are removed with the optimized approach of Szymkiewicz or by using the proposed MS1 and MS2 algorithms (Fig. 6b). The geometric average suffers from convergence difficulties. Its combination with the new technique provides satisfactory results. It should be noted that each average provides a particular solution, and the new algorithm differentiates itself from the upstream mean. Table 7 shows that Szymkiewicz's algorithm performs well for the different grid block sizes; the proposed algorithms give satisfactory results with comparable accu-

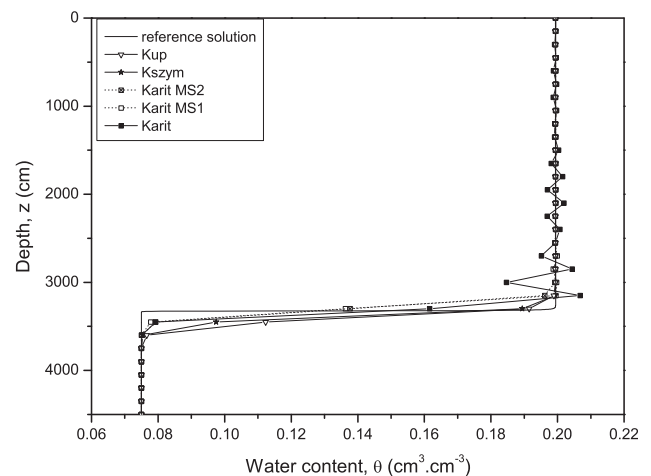


**Fig. 4.** Test case 1: profiles of water content at t = 30 h for the arithmetic mean, upstream mean, Darcian mean of Szymkiewicz (2009) and the new algorithms for a mesh size  $\Delta z = 150$  cm.

rary. According to Fig. 6a, arithmetic formulation exhibits large unphysical oscillations in the upper part of the domain. Hence, max ( $\Delta h/\Delta z$ ) is positive for the different grid sizes.

4.2.4. Test problem 4: evaporation with variable boundary condition

In this section, the algorithm presented by van Dam and Feddes (2000) has been implemented to manage the top boundary

condition. For extreme events of evaporation (or infiltration), their procedure takes into account the capacity of the soil to exfiltrate (or infiltrate) water with a prescribed potential flux. Hence, to avoid unphysical very large suction in case of prolonged dry weather or soil conditions, a dirichlet pressure head condition is imposed at the soil surface to govern the evaporation instead of the prescribed flux. Similarly, in case of too wet weather or soil conditions, the height of ponding is fixed and then regulates the infiltration in the soil profile. For the test problem 4 a constant evaporation rate of 0.5 cm/d is applied at the surface. When the suction at the first node reaches 137 700 cm the pressure head is maintained at this critical value. The lower pressure head boundary condition is maintained at the initial value. Simulations are performed during 5 days.

In a first time, the example of van Dam and Feddes (2000) has been simulated. A sand soil corresponding to soil 11 in Table 6 is selected and the initial condition corresponds to a uniform saturation ( $\theta/\theta_s$ ) of 44.4%. The cumulative evaporation ( $Q_{ev}$ ) and the time to drying ( $t_d$ ) are close to the results reported by Szymkiewicz (2009). Then, a soil column of 500-cm-deep is considered. The soil layer, the initial saturation condition and the mesh size are changed to test the monotonicity of the numerical method using different conductivity averaging techniques. Hence, for the sand soil used by van Dam and Feddes (2000) (soil no. = 11 in Table 6), monotonic solutions are obtained except with the combination of the arithmetic average, an initial pressure head of value  $h_{init} = -11$  cm and a nodal spacing of 50 cm. Initial saturations equal or greater than 45% for the soil no. = 1 lead to unphysical oscillations when using the arithmetic mean (with  $\Delta z \geq 5$  cm) or geometric mean (with  $\Delta z \geq 10$  cm). For the sandy loam no. 2, the critical initial saturation is around 73%. For  $h_{ini} = -14$  cm and  $\Delta z \geq 25$  cm, oscillations appear in the evaporation front both the arithmetic and geometric averages. Fig. 7 depicts the profiles of water content with a nodal spacing of 25 cm, an initial saturation of 45% and after 5 days of evaporation. Results differences due to the various conductivity averaging techniques can be observed at the surface of the column because of the variable boundary condition applied and also at the lower part of the soil profile. Arithmetic and geometric means exhibit large oscillations contrarily to the upstream mean, the optimized algorithm of Szymkiewicz (2009) and the switching algorithm MS1 which produce monotonic solutions. This trend has been confirmed for the numerous simulations performed with different types of soil, mesh sizes and initial condition. The cumulative evaporation ( $Q_{ev}$ ) and the time to drying ( $t_d$ ) are

reported in Table 8. These results show that the switching algorithm MS1 provides separate solutions of the upstream mean.

4.2.5. Test problem 5: 2D infiltration in an initially dry sand soil

For multidimensional problems, only a few studies have investigated the effect of the equivalent conductivity on the monotonicity and/or accuracy (for instance, Forsyth and Kropinski, 1997; Szymkiewicz and Burzyński, 2011). This problem is studied to evaluate the new algorithm in 2D. We consider a domain of 3 m wide by 3 m deep constituted by sand (soil no. = 1 in Table 6) and characterized by the modified van Genuchten model with an air entry pressure of 2 cm. The medium is initially dry ( $h_{init} = -1000$  cm) and impermeable conditions are applied for all boundaries, except on the top left hand corner ( $0 \leq x \leq 2$  m and  $z = 0$  m) where the infiltration flux is fixed to  $Q = 2.5$  m/day. The infiltration process occurs over 7 days, and the time step size varies heuristically between  $1 \times 10^{-3}$  s and 360 s.

For discretization consisting in quadrangular elements, two grids of 144 elements (25 cm  $\times$  25 cm) and 576 elements (12.5 cm  $\times$  12.5 cm) respectively are used. A fine grid solution has been computed by considering a 14,400-elements-mesh (2.5 cm  $\times$  2.5 cm). For rectangular elements, the M-matrix property cannot be verified (Belfort et al., 2009). Hence, this test case allows testing the ability of the different averaging techniques to produce monotonic results. For the computation of equivalent conductivity with the algorithm of Szymkiewicz (2009), a vertical

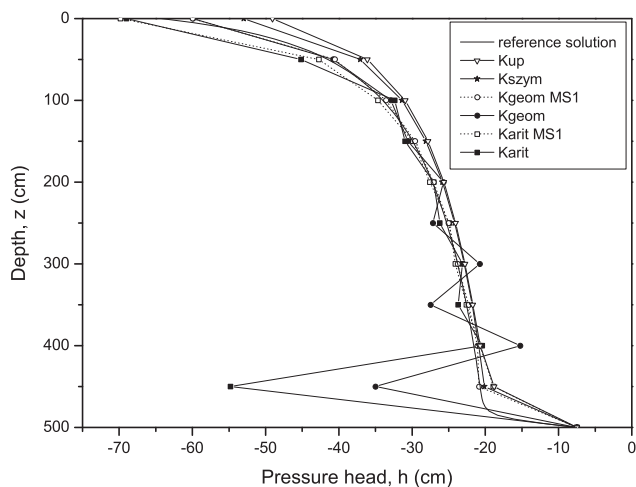


Fig. 5. Test case 2: pressure head profiles at time  $t = 30$  h for the drainage process in soil 5 obtained with different averaging methods and the proposed MS1 algorithm.

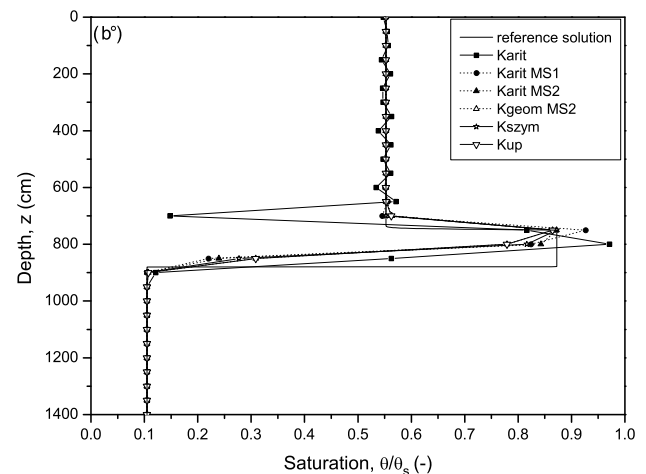
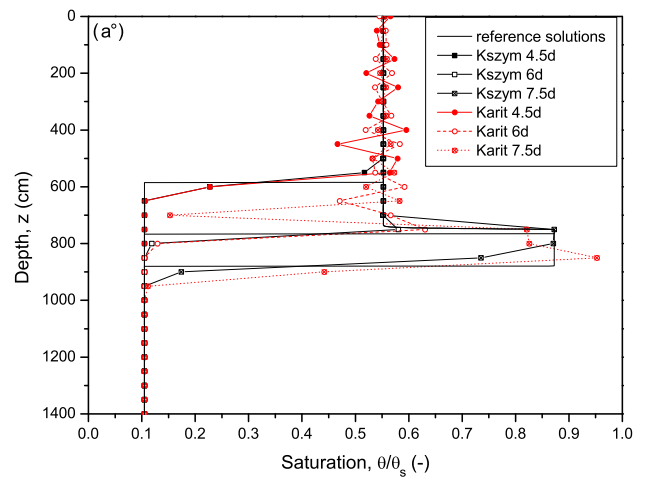
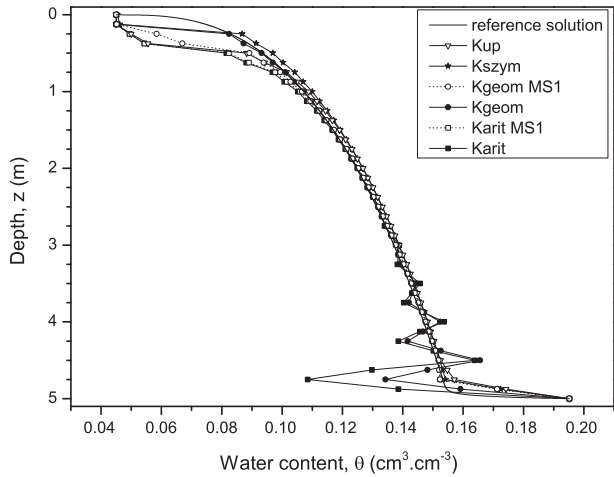
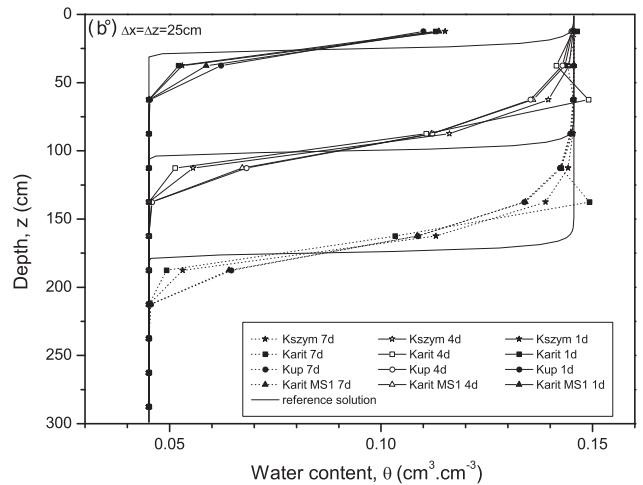
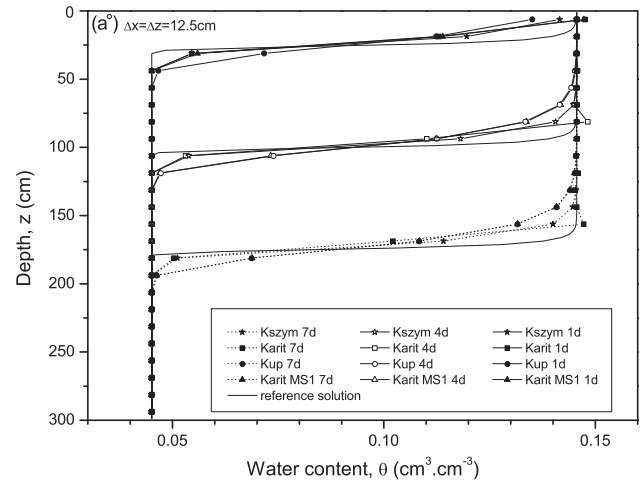


Fig. 6. Test case 3: saturation profiles obtained (a<sup>a</sup>) at different times with the standard averaging techniques and (b<sup>b</sup>) after 7.5 days of infiltration with the standard methods and the new algorithms.



**Fig. 7.** Test case 4: water content profiles obtained after 5 days of evaporation under variable upper boundary condition and with a nodal spacing of 25 cm.

conductivity is determined by using the one-dimensional optimized formulation (see appendix) and a horizontal conductivity is estimated with the integrated mean. These intermediate conductivities are computed with edges pressure head values. Since the MHFE method involves a single approximation per cell, the equivalent conductivity corresponds to the maximum of the two intermediate conductivities. Fig. 8 illustrates the water content profiles on a vertical segment located at  $x = 1$  m at different times. The arithmetic mean contains oscillations for both grid sizes at time equal to 4 and 7 days. The new algorithm removes these unphysical extremum. Additionally, it appears that the upstream formulation and optimized approach of Szymkiewicz are both free from oscillation.  $\theta$ -RMSE of the different solutions along the vertical segment are given in Table 9 at different times. The adaptation of the optimized algorithm runs and produces accurate results. Switching algorithm MS1 improves the accuracy of the solutions compared to upstream formulation and leads to specific solutions. With the coarser grid, the solutions obtained with  $K_{arit}$  MS1 and  $K_{up}$



**Fig. 8.** Test case 5: water content profiles (at the position  $x = 100$  cm) after 1–4 and 7 days of infiltration for lumped MHFE formulations and various averages. (a<sup>o</sup>) Refers to the grid of 576 elements and (b<sup>o</sup>) to the grid of 144 elements.

**Table 8**

Results of numerical simulations for test case 4 after 5 days of evaporation:  $Q_{ev}$  the cumulative evaporation and  $t_d$  the time to drying.

	$\Delta z = 25$ cm		$\Delta z = 50$ cm		
	$Q_{ev}$ (m)	$t_d$ (d)	$Q_{ev}$ (m)	$t_d$ (d)	
Kup	2.385E-02	4.551E+00	2.500E-02	>5	
Kszym	9.411E-03	1.895E+00	1.870E-02	3.760E+00	
Kgeom MS1	1.762E-02	1.635E+00	2.485E-02	4.189E+00	
Kgeom	8.099E-03	1.635E+00	1.520E-02	3.060E+00	
Karit MS1	2.034E-02	3.518E+00	2.500E-02	>5	
Karit	1.899E-02	3.441E+00	2.500E-02	>5	
		$\Delta z = 5$ cm		$\Delta z = 10$ cm	
Kup	8.951E-03	1.340E+00	1.341E-02	2.196E+00	
Kszym	2.859E-03	4.921E-01	4.283E-03	8.019E-01	
Kgeom MS1	2.470E-03	4.955E-01	6.043E-03	7.692E-01	
Kgeom	2.470E-03	4.955E-01	3.845E-03	7.692E-01	
Karit MS1	7.578E-03	1.132E+00	1.134E-02	1.758E+00	
Karit	7.570E-03	1.132E+00	1.092E-02	1.758E+00	
		$\Delta z = 1$ mm		$\Delta z = 1$ cm	
Kup	3.429E-03	3.204E-01	4.757E-03	5.771E-01	
Kszym	8.639E-04	2.156E-01	1.625E-03	3.117E-01	
Kgeom MS1	7.088E-04	2.134E-01	1.465E-03	2.927E-01	
Kgeom	7.088E-04	2.134E-01	1.465E-03	2.927E-01	
Karit MS1	3.317E-03	3.023E-01	4.253E-03	5.092E-01	
Karit	3.317E-03	3.023E-01	4.253E-03	5.107E-01	

**Table 9**

Error computation for the 2D test case:  $\theta$ -RMSE $_{\Delta z}$  along the vertical segment ( $x = 1$  m) for the different conductivity averaging methods and the switching algorithm MS1 at different times during the simulation.

	$\Delta x = \Delta z = 12.5$ cm		
	1 day	4 days	7 days
Karit	5.82E-03	6.14E-03	7.32E-03
Kszym	4.62E-03	4.73E-03	5.07E-03
Kup	8.07E-03	8.42E-03	8.25E-03
Karit MS1	5.74E-03	8.31E-03	8.24E-03
$\Delta x = \Delta z = 25$ cm			
Karit	9.39E-03	1.01E-02	1.20E-02
Kszym	8.82E-03	8.89E-03	9.53E-03
Kup	1.12E-02	1.19E-02	1.22E-02
Karit MS1	9.76E-03	1.17E-02	1.22E-02

are close to each other, mainly at the finale time due to the enlargement of the wetting front and the monotonicity difficulties.

The test case has also been solved with a discretization into triangular elements. A mesh of 225 triangles allows us to study the different formulations compared to a fine mesh solution obtained with 7419 elements. The optimized algorithm is adapted on each cell also by computing to intermediate conductivities. The first step consists in selecting the two edges where the piezometric head is maximum and minimum. Then, Szymkiewicz's formulation is

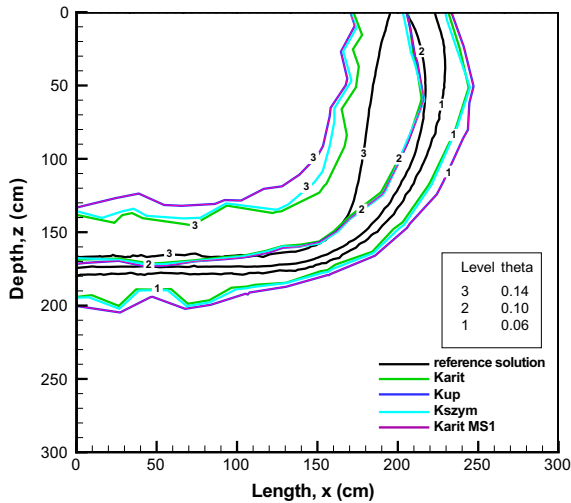


Fig. 9. Test case 5: isolines of water content obtained after 7 days of infiltration on triangular meshes with the different averaging techniques.

applied by considering the projection of these two points along the vertical axis. The second intermediate conductivity is the integrated mean constrained by both selected pressure head edge values. The maximum value is kept as the cell equivalent conductivity. If the selected points have the same height, only the second intermediate value is computed. Fig. 9 depicts isolines results obtained after 7 days of infiltration. During the simulation on the coarse grid, the arithmetic formulation provides oscillations and then the upstream mean and the switching algorithm MS1 give rather similar results.

## 5. Summary and conclusions

This study focuses on the issue of monotonicity when solving variably saturated flow problems modeled by the non-linear RE. Instead of specifically considering the M-matrix property, the criteria developed by Forsyth and Kropinski (1997) has been used to investigate the monotonicity because it also takes into account the conductivity-averaging method. In the first part of the article, different estimations of  $K_{eq}$  have been presented, including the Darcian mean approximation and optimized algorithm based on the importance of the gravity force (Baker, 2006; Szymkiewicz, 2009). Then, we demonstrate that the integrated formulation remains free from oscillation in the horizontal direction. This result corroborates the conclusion of Pei et al. (2012). The criterion of Forsyth and Kropinski (1997) shows that the upstream method would be the unique unconditional monotonic formulation. We demonstrate that the optimized algorithm developed by Szymkiewicz (2009) satisfy the monotonicity condition for infiltration. To conclude the theoretical part of the study, two switching algorithms are proposed. Both apply the upstream mean if a monotonicity test is not fulfilled during the iterative process for the solution produced by the chosen formulation. In the first approach (MS1), we verify that no unphysical extremum appears in the interior homogeneous part of the domain (without sink/source term). The second algorithm (MS2) adapts the conductivity in function of Forsyth and Kropinski's condition (Eq. (8) (b)).

Various numerical test cases using different material properties, flow conditions and grid sizes are solved. The following concluding remarks can be formulated:

- The M-matrix criterion is not sufficient to guaranty monotonicity, and the derivatives of the final matrix system have to be taken into account, which yields a condition dependent on the

estimation of the conductivity. This statement holds true for all numerical methods and is not specific to finite volume approach.

- Only the upstream formulation satisfies the monotonicity condition for all tested situations. In fact, by comparing our two algorithms, we show that the criterion of Forsyth and Kropinski (1997) is sufficient but not necessary. On the one hand, the use of the upstream mean is reduced with the first approach (MS1) compared to the second one (MS2). On the other hand, punctual applications of the upstream mean allow to “stabilize” the solution.
- The deficiencies of traditional averaging techniques have been observed mainly when the nodal spacing increases. Because the upstream formulation is often considered as a diffusive technique, our algorithms represent an alternative solution. Szymkiewicz's algorithm gives very efficient results; oscillation-free solutions have been obtained during the iterative process and not only at selected printing times.
- MS1 algorithm has been implemented in a 2D lumped MHFE method and tested on rectangular and triangular meshes. An adaptation of the optimized algorithm for MHFE equivalent conductivity has also been developed. Preliminary results are satisfactory and avoid unphysical oscillations.

The optimized algorithm developed by Szymkiewicz (2009) is a suitable technique to adapt automatically the conductivity in function of the considered 1D unsaturated flow problem. This technique prevents the development of unphysical oscillations in the solutions of all the test cases performed. Nonetheless, a generalization to different numerical methods in 2D and 3D can be challenging especially for complex/anisotropic geometries (Szymkiewicz, 2013). Beyond the interest of using our switching algorithm MS1 to investigate the issue of monotonicity and relativize the necessity of satisfying the monotonicity criterion of Forsyth and Kropinski (1997), its possible implementation in any numerical code makes it a suitable safety subroutine to avoid oscillations.

## Appendix A. Description and motonicity analysis of Szymkiewicz's algorithm

### A.1. Presentation of the algorithm and modification

Szymkiewicz (2009) considers that the parameter  $\chi$  which represents the cosine of the angle between the  $z$  axis and the direction of the gravity force is positive. It means that the angle should be comprised between  $-\pi/2$  and  $\pi/2$ . Hence, the algorithm has to be modified to handle all the situations encountered when using a computational code. For instance, a positive upward vertical  $z$  axis would lead to numerical difficulties (see description in Fig. 2) and the following modifications will be appreciated.

Notations:  $\Delta h = \Delta h_{ji} = h_j - h_i$ ,  $\Delta z = \Delta z_{ji} = z_j - z_i$ ,  $U$  (respectively  $L$ ) refers to upper (respectively lower) node.

#### Preliminary: variable ordering to identify upper and lower nodes

if ( $\chi \Delta z > 0$ ) then

$$h_U = h_i$$

$$h_L = h_j$$

else

$$h_U = h_j$$

$$h_L = h_i$$

end if

$$K_U = K(h_U)$$

**Case 0: Horizontal flow**

if ( $\chi = 0$ ) then  
if ( $\Delta h = 0$ ) then

$$K_{eq} = K_U$$

else

$$K_{eq} = [h_i - h_j]^{-1} \cdot \int_{h_j}^{h_i} K(h) \cdot dh$$

end if

return  
end if

**Case 1: Uniform or hydrostatic distribution**

if ( $\Delta h = 0$  or  $\Delta h = \chi \Delta z$ ) then

$$K_{eq} = K_U$$

**Case 2: Downward flow**

**Situation 1: Infiltration**

else if ( $\frac{\Delta h}{\chi \Delta z} < 0$ ) then

$K_{eq} = \max(K_1, K_2)$  with

$$\begin{cases} K_1 = \begin{cases} [h_U - h_L]^{-1} \cdot \int_{h_L}^{h_U} K(h) \cdot dh & \text{if } h_L \neq h_U \\ K(h_U) & \text{if } h_L = h_U \end{cases} \\ K_2 = \frac{\chi K_U}{\chi - \frac{\Delta h}{\Delta z}} \end{cases} \quad (A.1)$$

**Situation 2: Drainage**

else if ( $\frac{\Delta h}{\chi \Delta z} < 1$ ) then

$$K_{eq} = \min(K_1, K_2) \text{ with } \begin{cases} K_1 = \frac{\chi K_U}{\chi - \frac{\Delta h}{\Delta z}} \\ K_2 = K \left( h_L - \frac{\Delta h^2}{|\chi \Delta z|} \right) \end{cases} \quad (A.2)$$

**Case 3: Upward flow (Capillary rise)**

else

$$K_{eq} = \frac{|\Delta z| \times K_1 \times K_2}{[ (|\Delta z| - \Delta z_1) \times K_1 + \Delta z_1 \times K_2 ]}$$

with

$$K_1 = [(h_L - |\chi \Delta z|) - h_U]^{-1} \cdot \int_{h_U}^{h_L - |\chi \Delta z|} K(h) \cdot dh$$

$$K_2 = K(h_L - |\chi \Delta z|)$$

$$\Delta z_1 = \frac{\sqrt{\Delta h^2 + 4 \times \left( \frac{K_2}{K_1} - 1 \right) \times \chi \times (\Delta h - \chi \Delta z) \times \Delta z - |\Delta h|}}{2 \times |\chi| \times \left( \frac{K_2}{K_1} - 1 \right)}$$

end if

**A.2. Monotonicity analysis**

In this section, we consider that the upper node (subscript  $U$ ) can be either node  $j$  or node  $i$  and, to simplify the presentation, we assume that the M-matrix criterion is fulfilled ( $\gamma_{ij} \leq 0$ ).

**For infiltration problem:**

When using expression  $K_2$  of Eq. (1), we obtain Eq. (3) which is always negative.

Notice that two expressions can be distinguished (subscripts  $U$  and  $L$  identify the upper and lower nodes respectively):

$$\begin{cases} \text{if } h_j = h_L \text{ then } \gamma_{ij} K_s \frac{\partial K_{r,eq}}{\partial h_j^{n+1}} (H_j^{n+1} - H_i^{n+1}) + A_{ij}^{n+1} = 0 \\ \text{if } h_j = h_U \text{ then } \gamma_{ij} K_s \frac{\partial K_{r,eq}}{\partial h_j^{n+1}} (H_j^{n+1} - H_i^{n+1}) + A_{ij}^{n+1} = \gamma_{ij} K_s \chi \Delta z_{ij} \frac{\partial K_j}{\partial h_j} \end{cases} \quad (A.3)$$

Besides, expression  $K_1$  in Eq. (A.1) leads to the following expression:

$$\gamma_{ij} K_s \frac{\partial K_{r,eq}}{\partial h_j^{n+1}} (H_j^{n+1} - H_i^{n+1}) + A_{ij}^{n+1} = \gamma_{ij} K_s \left[ K_j - \frac{\chi \Delta z_{ji}}{\Delta h_{ji}} (K_j - K_{r,eq}) \right] \leq 0 \quad (A.4)$$

Which is conditionally negative. Actually, monotonicity of this expression would require:

$$\left[ K_j - \frac{\chi \Delta z_{ji}}{\Delta h_{ji}} (K_j - K_{r,eq}) \right] \geq 0 \quad (A.5)$$

For infiltration, i.e.  $\frac{\Delta h}{\chi \Delta z} < 0$ , Eq. (A.5) implies:

$$K_{r,eq} = \frac{1}{\Delta h_{ji}} \int_{h_i}^{h_j} K(h) dh \leq K_j \left( 1 - \frac{\Delta h_{ji}}{\chi \Delta z_{ji}} \right) \quad (A.6)$$

If  $j$  corresponds to the lower node and for a large nodal spacing, the integrated formulation can violate Eq. (A.6).

In Szymkiewicz (2009), since  $K_{eq}$  corresponds to the maximum of  $K_1$  and  $K_2$ , we demonstrate that the monotonicity condition is therefore fulfilled.

$$\gamma_{ij} K_s \frac{\partial K_{r,eq}}{\partial h_j^{n+1}} (H_j^{n+1} - H_i^{n+1}) + A_{ij}^{n+1} = \gamma_{ij} K_s \left[ K_j - \frac{\chi \Delta z_{ji}}{\Delta h_{ji}} (K_j - K_{r,eq}) \right]$$

Since the hydraulic interblock conductivity is computed from Eq. (A.1), we expect:

$$K_{r,eq} \geq \frac{\chi K_U}{\chi - \frac{\Delta h}{\Delta z}} \text{ and then:}$$

$$K_s \frac{\partial K_{r,eq}}{\partial h_j^{n+1}} (H_j^{n+1} - H_i^{n+1}) + K_s K_{r,eq} \geq K_s \left[ K_j - \frac{\chi \Delta z_{ji}}{\Delta h_{ji}} \left( K_j - \frac{\chi K_U}{\chi - \frac{\Delta h}{\Delta z}} \right) \right] \quad (A.7)$$

Using  $K_U \geq K_j$  in Eq. (A.7) leads to:

$$\begin{aligned} K_s \frac{\partial K_{r,eq}}{\partial h_j^{n+1}} (H_j^{n+1} - H_i^{n+1}) + K_s K_{r,eq} &\geq K_s K_j \left[ 1 - \frac{\chi \Delta z_{ji}}{\Delta h_{ji}} \left( 1 - \frac{\chi}{\chi - \frac{\Delta h}{\Delta z}} \right) \right] \\ &= K_s K_j \left[ 1 + \frac{1}{1 - \frac{\Delta h}{\chi \Delta z}} \right] \end{aligned} \quad (A.8)$$

Since  $\frac{\Delta h}{\chi \Delta z} < 0$  then Eq. (A.8) gives:

$$\gamma_{ij} K_s \frac{\partial K_{r,eq}}{\partial h_j^{n+1}} (H_j^{n+1} - H_i^{n+1}) + A_{ij}^{n+1} < 0$$

Consequently, the expression of Eq. (A.1) should respect the monotonicity condition of Eq. (8).

**For drainage problem:**

As mentioned for the infiltration case, using expression  $K_2$  of Eq. (A.2) allows to satisfy the monotonicity condition.

If  $K_{r,eq} = K \left( h_L - \frac{\Delta h_{ij}^2}{|\chi \Delta z_{ij}|} \right) = K(h_{eq})$ , the following equation can be deduced:

$$\begin{cases} \text{if } h_j = h_L \text{ then} \\ \gamma_{ij} K_s \frac{\partial K_{r,eq}}{\partial h_j^{n+1}} (H_j^{n+1} - H_i^{n+1}) + A_{ij}^{n+1} = \gamma_{ij} K_s \left[ K_{r,eq} + (\Delta h_{ji} - \chi \Delta z_{ji}) \left( 1 - 2 \frac{\Delta h_{ij}}{|\chi \Delta z_{ij}|} \right) \frac{\partial K_{r,eq}}{\partial h_{ij}} \right] \\ \text{if } h_j = h_U \text{ then} \\ \gamma_{ij} K_s \frac{\partial K_{r,eq}}{\partial h_j^{n+1}} (H_j^{n+1} - H_i^{n+1}) + A_{ij}^{n+1} = \gamma_{ij} K_s \left[ K_{r,eq} + 2 \frac{\Delta h_{ij}}{|\chi \Delta z_{ij}|} (\Delta h_{ji} - \chi \Delta z_{ji}) \frac{\partial K_{r,eq}}{\partial h_{ij}} \right] \end{cases} \quad (A.9)$$

For  $h_j = h_L$ , it appears that the sign of Eq. (A.9) depends on the values of the conductivity and its derivative, specifically when  $0 \leq \Delta h_{ji} < \frac{|\Delta z_{ji}|}{2}$ .

$K_{eq}$  corresponds to the minimum of  $K_1$  and  $K_2$  (Eq. (A.2)), but contrarily to infiltration case, it is not possible to establish the monotonicity of the scheme.

Hence, these theoretical developments are completed by numerical investigations.

## References

- An, H., Ichikawa, Y., Tachikawa, Y., Shiiba, M., 2011. A new Iterative Alternating Direction Implicit (IADI) algorithm for multi-dimensional saturated-unsaturated flow. *J. Hydrol.* 408 (1–2), 127–139.
- Baker, D.L., 1995. Darcian weighted interblock conductivity means for vertical unsaturated flow. *Ground Water* 33 (3), 385–390.
- Baker, D.L., 2000. A Darcian integral approximation to interblock hydraulic conductivity means in vertical infiltration. *Comput. Geosci.* 26 (5), 581–590.
- Baker, D.L., 2006. General validity of conductivity means in unsaturated flow models. *J. Hydrol. Eng.* 11 (6), 526–538.
- Baker, D.L., Arnold, M.E., Scott, H.D., 1999. Some analytical and approximate Darcian means. *Ground Water* 37 (4), 532–538.
- Belfort, B., Carrayrou, J., Lehmann, F., 2007. Implementation of Richardson extrapolation in an efficient adaptive time stepping method: applications to reactive transport and unsaturated flow in porous media. *Trans. Porous Media* 69 (1), 123–138.
- Belfort, B., Lehmann, F., 2005. Comparison of equivalent conductivities for numerical simulation of one-dimensional unsaturated flow. *Vadose Zone J.* 4 (4), 1191–1200.
- Belfort, B., Ramasomanana, F., Younes, A., Lehmann, F., 2009. An efficient lumped mixed hybrid finite element formulation for variably saturated groundwater flow. *Vadose Zone J.* 8 (2), 352–362.
- Brooks, R.H., Corey, A.T., 1964. Hydraulic properties of porous media. *Hydrol. Pap.* 3, Colo. State Univ., Fort Collins.
- Brunone, B., Ferrante, M., Romano, N., Santini, A., 2003. Numerical simulations of one-dimensional infiltration into layered soils with the Richards' equation using different estimates of the interlayer conductivity. *Vadose Zone J.* 2 (2), 193–200.
- Carsel, R.F., Parrish, R.S., 1988. Developing joint probability distribution of soil water retention characteristics. *Water Resour. Res.* 24 (5), 755–769.
- Celia, M.A., Bouloutras, E.T., Zarba, R.L., 1990. A general mass conservative numerical solution for the unsaturated flow equation. *Water Resour. Res.* 26 (7), 1483–1496.
- Chavent, G., Roberts, J.E., 1991. A unified physical presentation of mixed, mixed hybrid finite elements and standard finite difference approximations for the determination of velocities in water flow problems. *Adv. Water Resour.* 14 (6), 329–348.
- Cooley, R.L., 1983. Some new procedures for numerical solution of variably saturated flow problems. *Water Resour. Res.* 19 (5), 1271–1285.
- Crevoisier, D., Chanzy, A., Voltz, M., 2009. Evaluation of the Ross fast solution of Richards' equation in unfavourable conditions for standard finite element methods. *Adv. Water Resour.* 32 (6), 936–947.
- Farthing, M.W., Kees, C.E., Miller, C.T., 2003. Mixed finite element methods and higher order temporal approximations for variably saturated groundwater flow. *Adv. Water Resour.* 26 (4), 373–394.
- Forsyth, P.A., Kropinski, M.C., 1997. Monotonicity considerations for saturated-unsaturated subsurface flow. *Siam J. Sci. Comput.* 18 (5), 1328–1354.
- Forsyth, P.A., Wu, Y.S., Pruess, K., 1995. Robust numerical methods for saturated-unsaturated flow with dry initial conditions in heterogeneous media. *Adv. Water Resour.* 18 (1), 25–38.
- Fuentes, C., Haverkamp, R., Parlange, J.-Y., 1992. Parameter constraints on closed-form soil–water relationships. *J. Hydrol.* 134 (1–4), 117–142.
- Gardner, W.R., 1958. Some steady-state solutions of the unsaturated moisture flow equation with application to evaporation from water table. *Soil Sci.* 85 (4), 228–232.
- Gastó, J.M., Grifoll, J., Cohen, Y., 2002. Estimation of internodal permeabilities for numerical simulation of unsaturated flows. *Water Resour. Res.* 38 (12), 1326.
- Haverkamp, R., Vauclin, M., 1979. A note on estimating finite difference interblock hydraulic conductivity values for transient unsaturated flow problems. *Water Resour. Res.* 15 (1), 181–187.
- Haverkamp, R., Vauclin, M., Touma, J., Wierenga, P.J., Vachaud, G., 1977. A comparison of numerical simulation models for one-dimensional infiltration. *Soil Sci. Soc. Am. J.* 41 (2), 285–294.
- Hoteit, H., Mose, R., Philippe, B., Ackerer, P., Erhel, J., 2002. The maximum principle violations of the mixed-hybrid finite-element method applied to diffusion equations. *Int. J. Numer. Methods Eng.* 55 (12), 1373–1390.
- Huyakorn, T., Thompson, S., Thompson, B., 1984. Techniques for making finite element methods competitive in modelling flow in variably saturated porous media. *Water Resour. Res.* 20 (8), 1099–1115.
- Ippisch, O., Vogel, H.-J., Bastian, P., 2006. Validity limits for the van Genuchten–Mualem model and implications for parameter estimation and numerical simulation. *Adv. Water Resour.* 29 (12), 1780–1789.
- Ju, S.-H., Kung, K.-J.S., 1997. Mass types, element orders and solution schemes for the Richards equation. *Comput. Geosci.* 23 (2), 175–187.
- Karthikeyan, M., Tan, T.S., Phoon, K.K., 2001. Numerical oscillation in seepage analysis of unsaturated soils. *Can. Geotech. J.* 38 (3), 639–651.
- Kuráž, M., Mayer, P., Lepš, M., Trpkošová, D., 2010. An adaptive time discretization of the classical and the dual porosity model of Richards' equation. *J. Comput. Appl. Math.* 233 (12), 3167–3177.
- Lassabatere, L., Angulo-Jaramillo, R., Soria Ugalde, J.M., Cuenca, R., Braud, I., Haverkamp, R., 2006. Beerkan estimation of soil transfer parameters through infiltration experiments—BEST. *Soil Sci. Soc. Am. J.* 70 (2), 521–532.
- Lehmann, F., Ackerer, Ph., 1998. Comparison of iterative methods for improved solutions of the fluid flow equation in partially saturated porous media. *Trans. Porous Media* 31 (3), 275–292.
- Lott, P.A., Walker, H.F., Woodward, C.S., Yang, U.M., 2012. An accelerated Picard method for nonlinear systems related to variably saturated flow. *Adv. Water Resour.* 38, 92–101.
- Loudy, D., Falconer, R.A., Lin, B., 2007. Mathematical development and verification of a non-orthogonal finite volume model for groundwater flow applications. *Adv. Water Resour.* 30 (1), 29–42.
- Manzini, G., Ferraris, S., 2004. Mass-conservative finite volume methods on 2-D unstructured grids for the Richards' equation. *Adv. Water Resour.* 27 (12), 1199–1215.
- Miller, C.T., Williams, G.A., Kelley, C.T., Tocci, M.D., 1998. Robust solution of Richards' equation for nonuniform porous media. *Water Resour. Res.* 34 (10), 2599–2610.
- Milly, P.C.D., 1985. A mass-conservative procedure for time-stepping models of unsaturated flow. *Adv. Water Resour.* 8 (1), 32–36.
- Neuman, S.P., 1972. Finite element computer programs for flow in saturated-unsaturated porous media. Second annual report, A10-SWC-77, Hydraul. Eng. Lab., Technion, Haifa, Israël.
- Oldenburg, C.M., Pruess, K., 1993. On numerical modeling of capillary barriers. *Water Resour. Res.* 29 (4), 1045–1056.
- Pan, L., Warrick, A.W., Wierenga, P.J., 1996. Finite element methods for modeling water flow in variably saturated porous media: numerical oscillation and mass-distributed schemes. *Water Resour. Res.* 32 (6), 1883–1889.
- Pei, Y.S., Yang, Z.F., Zhang, K.J., Tian, B.H., 2012. Deficiency of approximate interblock conductivities for simulation of horizontal unsaturated flow. *Transp. Porous Media* 91, 627–647.
- Rathfelder, K., Abriola, L.M., 1994. Mass conservative numerical solutions of the head-based Richards equation. *Water Resour. Res.* 30 (9), 2579–2586.
- Rawls, W.J., Brakensiek, D.L., Saxton, K.E., 1982. Estimation of soil water properties. *Trans. ASAE* 25 (5), 1316–1320.
- Romano, N., Brunone, B., Santini, A., 1998. Numerical analysis of onedimensional unsaturated flow in layered soils. *Adv. Water Resour.* 21 (4), 315–324.
- Russo, D., 1988. Determining soil hydraulic properties by parameter estimation: On the selection of a model for hydraulic properties. *Water Resour. Res.* 24 (3), 453–459.
- Sandhu, R.S., Liu, H., Singh, K.J., 1977. Numerical performance of some finite element schemes for analysis of seepage in porous elastic media. *Int. J. Numer. Anal. Methods Geomech.* 1 (2), 177–194.
- Schaap, M.G., Leij, F.J., 2000. Improved prediction of unsaturated hydraulic conductivity with the Mualem–van Genuchten model. *Soil Sci. Soc. Am. J.* 64 (3), 843–851.
- Schnabel, R.R., Richie, E.B., 1984. Calculation of internodal conductances for unsaturated flow simulations: a comparison. *Soil Sci. Soc. Am. J.* 48 (5), 1006–1010.
- Schweizer, B., 2012. The Richards equation with hysteresis and degenerate capillary pressure. *J. Differ. Equations* 252 (10), 5594–5612.
- Šimůnek, J., Bradford, S.A., 2008. Vadose zone modeling: introduction and importance. *Vadose Zone J.* 7, 581–586.
- Šimůnek, J., van Genuchten, M.Th., Šejna, M., 2006. The HYDRUS Software Package for Simulating the Two- and Three-Dimensional Movement of Water, Heat, and Multiple Solutes in Variably-Saturated Media. Technical manual version 1.0, 213p.
- Srivastava, R., Yeh, T.-C.J., 1991. Analytical solutions for one-dimensional, transient infiltration toward the water table in homogeneous and layered soils. *Water Resour. Res.* 27 (5), 753–762.
- Szymkiewicz, A., 2009. Approximation of internodal conductivities in numerical simulation of one-dimensional infiltration, drainage, and capillary rise in unsaturated soils. *Water Resour. Res.* 45, W10403. <http://dx.doi.org/10.1029/2008WR007654>.
- Szymkiewicz, A., 2013. Modelling Water Flow in Unsaturated Porous Media. Springer, Berlin Heidelberg.
- Szymkiewicz, A., Burzyński, K., 2011. Computing internodal conductivities in numerical modeling of two dimensional unsaturated flow on rectangular grid. *Archives Civil Eng.* 57 (2), 215–225.
- Szymkiewicz, A., Helmig, R., 2011. Comparison of conductivity averaging methods for one-dimensional unsaturated flow in layered soils. *Adv. Water Resour.* 34 (8), 1012–1025.
- Szymkiewicz, A., Lewandowska, J., Angulo-Jaramillo, R., Butlańska, J., 2008. Two-scale modeling of unsaturated water flow in a double-porosity medium under axisymmetric conditions. *Can. Geotech. J.* 45, 238–251.
- Thomas, H.R., Zhou, Z., 1997. Minimum time-step size for diffusion problem in FEM analysis. *Int. J. Numer. Methods Eng.* 40, 3865–3880.
- van Dam, J.C., Feddes, R.A., 2000. Numerical simulation of infiltration, evaporation and shallow groundwater levels with the Richards equation. *J. Hydrol.* 233 (1–4), 72–85.

- van Genuchten, M.Th., 1980. A closed-form equation for predicting the hydraulic conductivity of unsaturated soils. *Soil Sci. Soc. Am. J.* 44 (5), 892–898.
- Vermeer, P.A., Verruijt, A., 1981. An accuracy conditions for consolidation by finite elements. *Int. J. Numer. Anal. Methods Geomech.* 5 (1), 1–14.
- Vogel, T., van Genuchten, M.Th., Cislerova, M., 2001. Effect of the shape of the soil hydraulic functions near saturation on variably saturated flow predictions. *Adv Water Resour.* 24 (2), 133–144.
- Warrick, A.W., 1991. Numerical approximation of Darcian flow through unsaturated soil. *Water Resour. Res.* 27 (6), 1215–1222.
- Windisch, G., 1989. *M-Matrices in Numerical Analysis*. Teubner-Texte zur Mathematik, 139p.
- Wood, W.L., 1996. A note on how to avoid spurious oscillation in the finite-element solution of the unsaturated flow equation. *J. Hydrol.* 176 (1–4), 205–218.
- Wu, M., 2010. A finite-element algorithm for modeling variably saturated flows. *J. Hydrol.* 394 (3–4), 315–323.
- Younes, A., Ackerer, Ph., Lehmann, F., 2006. A new mass lumping scheme for the mixed hybrid finite element method. *Int. J. Numer. Methods Eng.* 67 (1), 89–107. <http://dx.doi.org/10.1002/nme.1628>.
- Zadeh, K.S., 2011. A mass-conservative switching algorithm for modeling fluid flow in variably saturated porous media. *J. Comput. Phys.* 230 (3), 664–679.
- Zaidel, J., Russo, D., 1992. Estimation of finite difference interblock conductivities for simulation of infiltration into initially dry soils. *Water Resour. Res.* 28 (9), 2285–2295.
- Zambra, C.E., Dumbser, M., Toro, E.F., Moraga, N.O., 2012. A novel numerical method of high-order accuracy for flow in unsaturated porous media. *Int. J. Numer. Methods Eng.* 89, 227–240.